Extreme Precipitation Changes in Europe from the Last Millennium to the End of the Twenty-First Century

RAN HUO

State Key Laboratory of Water Resources and Hydropower Engineering Science, and Hubei Provincial Key Lab of Water System Science for Sponge City Construction, Wuhan University, Wuhan, China

LU LI

NORCE Norwegian Research Centre, Bjerknes Centre for Climate Research, Bergen, Norway

HUA CHEN

State Key Laboratory of Water Resources and Hydropower Engineering Science, and Hubei Provincial Key Lab of Water System Science for Sponge City Construction, Wuhan University, Wuhan, China, and Department of Geography and Geographic Information Science, University of Illinois at Urbana–Champaign, Urbana, Illinois

CHONG-YU XU

Department of Geosciences, University of Oslo, Oslo, Norway

JIE CHEN AND SHENGLIAN GUO

State Key Laboratory of Water Resources and Hydropower Engineering Science, Wuhan University, Wuhan, China

(Manuscript received 26 November 2019, in final form 27 July 2020)

ABSTRACT: In this study, we aim to better understand the current and future projections of precipitation extremes in Europe in the context of climatic variability over a long-term period from the last millennium to the end of the twenty-first century. The daily gridded precipitation data from five global climate models (GCMs) of phase 5 of the Coupled Model Intercomparison Project (CMIP5) are chosen to investigate natural variability and precipitation extremes during the last millennium (850–1849), the historical (1850–2005) period, and two representative concentration pathway (RCP2.6 and RCP8.5) scenarios (2006–99). First, the seasonal and annual precipitation and extreme statistics from GCMs are evaluated using reconstruction and observation. Second, the spatial and temporal patterns of extreme precipitation from GCMs are investigated from the last millennium to the end of the twenty-first century. Meanwhile, the characteristic changes of extreme precipitation for the five regions of Europe are further analyzed. The results revealed the following: GCMs underestimate extreme precipitation and overestimate mean precipitation compared with the observations from European Climate Assessment and Dataset (ECA&D); the majority of Europe except southern Europe will most likely have large magnitude increases in the extreme precipitation and mean precipitation in the future under both RCP scenarios; there is no systematic change of precipitation extremes from the last millennium to the historical period from all GCMs; and larger magnitude increases are shown in 100- and 200-yr than in 5- and 10-yr return period precipitation from both RCP scenarios. In addition, short-duration extreme precipitation will most likely increase more than longer-duration extremes.

KEYWORDS: Europe; Climate change; Climate variability; Precipitation

1. Introduction

In recent decades, Europe has experienced a significant increase in hydrological extremes that have significantly impacted socioeconomic and natural systems. A series of recorded flood events have occurred, such as the disastrous August 2002 flood in central Europe and the devastating flood in Germany in 2013 (Ulbrich et al. 2003; Merz et al. 2014). However, such extreme events have long return periods and rarely appear in observational datasets (Hirabayashi et al. 2013). Thus, key challenges remain in understanding the characteristics of European precipitation extremes and their future changes (Beniston et al. 2007).

Most importantly, it is difficult to quantitatively assess the climatological significance of extreme events due to the high degree of natural hydroclimate variability and the limited length of observations. Europe is one of the few regions in the world with substantial coverage of long instrumental records, documentary evidence, and high-resolution spatiotemporally natural proxies. Previous studies have used historical precipitation documents and dense proxy records to infer climate variability in Europe at decadal to centennial time scales longer than the instrumental data record. For example, Pauling et al. (2006) presented seasonal precipitation reconstructions for

Denotes content that is immediately available upon publication as open access.

Correspondence authors: Hua Chen, chua@whu.edu.cn; Lu Li, luli@norceresearch.no

DOI: 10.1175/JCLI-D-19-0879.1

Europe covering the period 1500–1900 together with gridded reanalysis data from 1901 to 2000 based on documentary evidence and natural proxies (i.e., tree-ring chronologies, ice cores, corals, and a speleothem). They discovered that conditions during the Medieval Climate Anomaly (MCA) period (AD 900–1150; hereafter all dates are AD) were considerably wetter than today, while climate was dry during most of the ''Little Ice Age'' (LIA; 1500–1850), and these findings were also confirmed by Feurdean et al. (2015). In addition, it is worth noting that the divisions of the MCA and LIA periods vary in different regions. Such studies are an essential source of information necessary to understand climatic processes and variability. However, these approaches can only be applied in regions that have abundant multiproxy records with sufficient chronological control. Hence, it is necessary to adopt other approaches to understand the precipitation characteristics for the period prior to instrumental records, such as evaluating whether simulations from climate models and reconstructions from proxy data are compatible realizations of the unknown past climate evolution (Bothe et al. 2013; Klein et al. 2016). From this perspective, Shi et al. (2016) investigated the spatiotemporal characteristics of annual and seasonal rainfall changes from the MCA (950–1250) to the LIA (1500–1800) based on the last millennium simulations of phase 3 of the Paleoclimate Modeling Intercomparison Project (PMIP3). They examined the long-term variation of precipitation in arid central Asia and eastern China based on the PMIP3 last millennium simulations of nine models. In comparison with the reconstructions, they discovered that only one model, MRI-CGCM3, was able to broadly reproduce the reconstructed humidity pattern in Asia (Shi et al. 2016).

The CMIP5 GCMs provide a means for understanding the range of long-term natural variability and also yield future projections under the ongoing global warming scenario. Many studies, using various trend detection methods (Min et al. 2011; Westra et al. 2013) and datasets (Alexander et al. 2006; Donat et al. 2013; Kharin et al. 2007), have found that about two-thirds of the data-covered global land areas exhibit positive trends in precipitation extremes for the latter half of the twentieth century. Increasing trends in precipitation extremes were observed over many regions of Europe, notably for northern and eastern Europe, while decreases were observed in southern Europe (Donat et al. 2013; Groisman et al. 2005; Madsen et al. 2014; van den Besselaar et al. 2013). The detection of such trends in observational statistics is challenging, however, due to the substantial spatial and temporal variability of extreme events (Groisman et al. 2005). This has also been demonstrated by RCM projections in Europe (Rajczak and Schar 2017), which have revealed that the frequency or intensity of heavy precipitation events has likely increased over the past decade. Such a trend will presumably continue into the future, as indicated by modeling studies associated with EURO-CORDEX regional climate models (RCMs). For Europe, assessments of regional changes, impacts, and subsequent adaptation measures are often based on finer-resolved RCM ensembles (e.g., PRUDENCE and ENSEMBLES). For example, Fowler et al. (2007) used four models, including three RCMs from Prediction of Regional Scenarios and Uncertainties for Defining European Climate Change Risks and Effects (PRUDENCE) and an atmosphere-only GCM with a similar spatial resolution. By comparing return values for the current (1961–90) and future (2070–99) climates, they determined that in northern Europe, along with the increasing mean precipitation, extreme short-term precipitation events will possibly increase in both magnitude and frequency. In addition, Lehtonen et al. (2014) compared the control period simulations with the high-resolution ENSEMBLES observations (E-OBS v7.0)—a gridded observational precipitation dataset—in order to evaluate the performance of the models and explore seasonal changes in indices, such as the maximum 1-day precipitation and the maximum 5-day precipitation. They determined excessive or scarce precipitation in Europe based on simulations performed with 10 GCMs and, for comparison, with 5 RCMs driven by one GCM, which indicated that there will be a shift toward a climate with more extreme precipitation in Europe as greenhouse-gas-induced global warming continues. In addition, Scoccimarro et al. (2016) investigated possible changes in the distribution of heavy precipitation events in a warmer climate over the Euro-Mediterranean region, using the results of a set of 20 climate models taking part in CMIP5 under the representative concentration pathway (RCP) 8.5 scenario. Those GCMs indicated a stretching of the right tail of precipitation event distribution at the end of the twenty-first century, even over regions showing a decrease in the mean precipitation, which would correspond to strong increased availability of water vapor content in the atmospheric column in the future.

It is difficult, however, to evaluate the future projections of precipitation extremes and floods, given the high degree of natural variability, the anthropogenic forcing, and the limited instrumental measurements covering only the last 100 years. Rarely studies have examined the changes of extreme precipitation characteristics over a long-term period of more than 1000 years by combining the last millennium with a projection to the end of the twenty-first century. Schindler et al. (2015) analyzed the internal variability of daily precipitation for preindustrial simulation of a stationary climate based on one GCM of CMCC-CM. Their results implied that preindustrial precipitation from the climate model with 30 years seemed enough for characterizing the internal variability of daily precipitation in many regions (especially in the midlatitudes); however, some exceptions exist, which need 50 years or even more. They also recommended that climate simulations from more GCMs are needed in order to get a robust result. Ljungqvist et al. (2016) pointed out the divergence between reconstructed hydroclimatic anomalies and model output in the simulated intensification of hydroclimatic variability in the twentieth century, which suggested the use of paleoclimate data to place recent and predicted changes of hydrological extremes and trends in a millennium-long context.

In this study, we attempted to explore the characteristics and changes of precipitation extremes from the last millennium to the end of the twenty-first century in Europe due to the impact of past and projected anthropogenic climate change. Two major questions were addressed: 1) Could the last 100 years'

instrumental measurements (1900–present) represent precipitation variability and extreme statistics over a long-term period of more than 1000 years? 2) What are the projected changes of different levels of precipitation extremes (i.e., 5-, 10-, 20-, 50-, 100-, and 200-yr return) in Europe due to future anthropogenic climate change?

To answer the above questions, we used the daily precipitation from five CMIP5 GCMs over 1250 years, including the last millennium projections from 850 to 1849 (past1000), historical projections from 1850 to 2005 (historical), and future projections from 2006 to 2099 (RCP2.6 and RCP8.5). A series of extreme indices were chosen to comprehensively analyze and evaluate the characteristics of extreme precipitation in Europe, including annual maximum 1-, 5-, and 15-day precipitation totals corresponding to the 5-, 10-, 20-, 50-, 100-, and 200-yr return periods. In addition, we divided Europe into five regions according to their common geographical locations (https://www.mapsofworld.com/europe/), namely northern, southern, central, eastern, and western Europe, in order to facilitate a more detailed investigation and a discussion of uncertainty and spatial variability.

The organization of this manuscript is as follows. After this brief introduction, a description of the study area and data is presented, followed by the methods utilized. Next, the results of an evaluation of the CMIP5 GCMs' ability to simulate mean and extreme precipitation statistics, as well as the characteristics and changes of precipitation extremes over a 1000-yr period in Europe, are presented. This paper ends with a discussion followed by conclusions.

2. Study area and data description

a. Study area

Most of Europe lies in the temperate zone and is affected by the ocean. It is characterized by mild and rainy weather throughout the year. The annual precipitation in western Europe and the western part of northern Europe is distributed relatively homogeneously, varying between 600 and 1000 mm in most areas. Due to frequent cyclone activity in winter, precipitation is somewhat higher. In the eastern part of northern Europe, as well as central and eastern Europe, the greatest amount of precipitation occurs in the summer months due to the increased continentality. In southern Europe, due to the influence of both the polar front and the cyclone activity associated with the Mediterranean front, precipitation primarily occurs in winter, with anticyclonic dominance resulting in less precipitation in summer. Annual precipitation in this region is approximately 350–900 mm.

b. Data

1) CMIP5 MODELS AND EXPERIMENTS

In this study, the daily precipitation data from five GCMs in the CMIP5 were used (Table 1). The CMIP5 experiments including the last millennium simulations (past1000; 850–1849), the historical simulations (historical; 1850–2005), and the anthropogenically forced simulations of the twenty-first century (RCP2.6 and RCP8.5; 2006–99) are listed in Table 2.

TABLE 1. Basic information for the CMIP5 models selected for evaluation over the study area.

Model	Institute	Resolution (lat × lon)
BCC-CSM1.1	Beijing Climate Center, China	2.8° × 2.8°
MIROC-ESM	Atmosphere and Ocean Research Institute (The University of Tokyo), National Institute for Environmental Studies, and Japan Agency for Marine-Earth Science and Technology, Japan	2.8° × 2.8°
MPI-ESM-P	Max Planck Institute for Meteorology, Germany	1.9° × 1.9°
MRI-CGCM3	Meteorological Research Institute, Japan	1.125° × 1.125°
CCSM4	National Center for Atmospheric Research, U.S. Department of Energy/ National Science Foundation, United States	0.9° × 1.25°

The last millennium simulations have reconstructed time-evolving exogenously-imposed forcing. The historical simulations include changing anthropogenic and natural forcing factors, which are imposed to reproduce climate evolution through the twentieth century as accurately as possible. Two pathway scenarios, RCP2.6 and RCP8.5, are used in the paper for comparison. The radiative forcing in RCP8.5 (the high CO_2 concentrations scenario) increases throughout the twenty-first century before reaching a level of about 8.5 W m^{-2} at the end of the century (Peters et al. 2012; Lewis 2017). In addition to this "high" scenario, the RCP2.6 scenario is an aggressive mitigation trajectory, where the greenhouse gas emissions reach a maximum near the middle of the twenty-first century and then decline by the end of the twenty-first century (Dai et al. 2016). Both periods are from 2006 to 2099. The CMIP5 GCMs were used where data were available for all experiments, resulting in a significantly reduced number of available models (i.e., BCC-CSM1.1, MIROC-ESM, MPI-ESM-P, MRI-CGCM3, and CCSM4) compared to the total number of CMIP5 GCMs since few groups contributing to past1000 simulations were available. In addition, daily data from the MPI-ESM-P model are missing in the projection of the RCP2.6 and RCP8.5 scenarios from the CMIP5 archive.

2) PROXY PRECIPITATION DATA OF THE PAST1000 PERIOD

Millennium-long precipitation reconstructions based on documentary evidence and natural proxies such as tree-ring chronologies were used as reference data in this study. In Europe, the reconstructions of seasonal precipitation covering the period 1500–2000 (10°W–40°E and 35°–70°N; 0.5° × 0.5° resolved grid) were available (Pauling et al. 2006). The four seasons were defined as winter (December–February), spring (March–May), summer (June–August), and autumn (September–November).

TABLE 2. List of selected CMIP5 experiments with major imposed forcings and periods.

Experiment	Major imposed forcings	Years
Past1000	Volcanic aerosols, well-mixed greenhouse gases, land use, orbital parameters, and solar changes	850–1849
Historical	Anthropogenic (greenhouse gases, aerosols, ozone) and natural (solar, volcanic)	1850–2005
RCP2.6	Anthropogenic (greenhouse gases, aerosols, ozone scenarios) and natural (solar) forcings. Radiative forcing reaches a level of about 2.6 W m^{-2} at the end of the twenty-first century.	2006–99
RCP8.5	Anthropogenic (greenhouse gases, aerosols, and ozone scenarios) and natural (solar). Radiative forcing reaches a level of approximately 8.5 W m^{-2} by the end of the twenty-first century	2006–99

Due to the limitation of available reconstruction data, we can only compare the spatial distributions of seasonal precipitation between the CMIP5 GCMs and the reconstructed data.

3) HISTORICAL PRECIPITATION OBSERVATION

In this study, the performances of extreme precipitation simulations from the CMIP5 GCMs during the historical period were evaluated based on the station observations from the European Climate Assessment and Dataset (ECA&D) for 1922–2005 (https://eca.knmi.nl//dailydata/predefinedseries.php). The observed stations whose number of missing days exceeded 10% of the total number of days in the historical period were removed from the analysis in this investigation. After quality checking, 1402 stations were available for use over Europe, as shown in Fig. 1.

3. Methods

a. *Precipitation evaluation for the past1000 period*

To evaluate the performance of the CMIP5 GCMs for the past1000 period, we compared the past1000 simulations with the multiproxy reconstructed data. The spatial resolutions of the five chosen CMIP5 GCMs varied from (1.12° × 1.12°) to (2.8° × 2.8°), as listed in Table 1. Therefore, we regridded all the CMIP5 GCMs to the same grid size (1.0° × 1.0°) using bilinear interpolation (Jiang et al. 2015) for the past1000 evaluation for comparison with the reconstructed data, which were also regridded to the same resolution.

b. *Precipitation evaluation for the historical period*

To evaluate the performance of the CMIP5 GCMs for the historical period, we compared the historical simulations with the ECA&D station precipitation data. The CMIP5 GCMs gridded precipitation data were interpolated to the 1402 ECA&D observation stations using the inverse distance weighted (IDW) method for comparison consistency. Therefore, the calculations of the simulated and observed extreme indices were all station-based.

In addition, we divided the European continent into five regions according to common geographical divisions: northern Europe (NE), southern Europe (SE), central Europe (CE), eastern Europe (EE), and western Europe (WE). The area-averaged precipitation indices were likewise examined in order to obtain a more coherent picture of the projected changes. In this part of the comparison, the values of simulated and

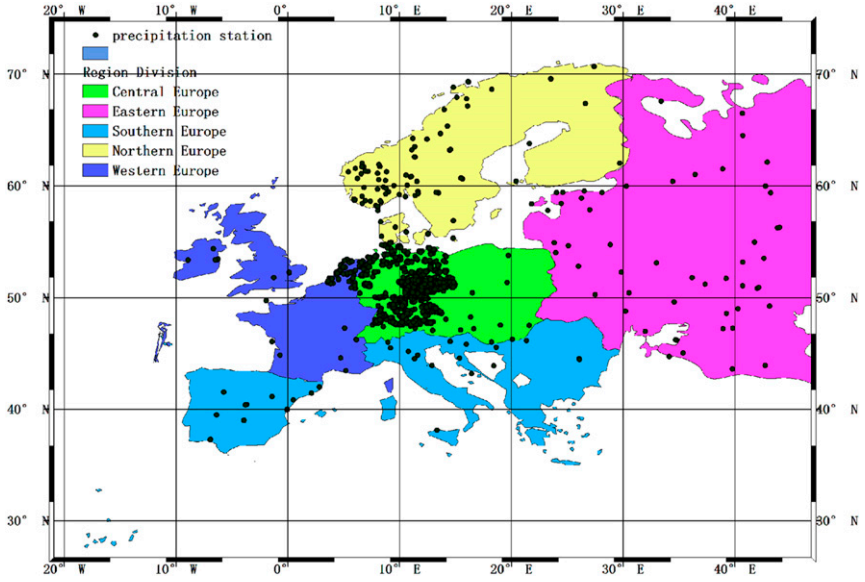

FIG. 1. Spatial distribution of the chosen 1402 observation rain gauges from the ECA&D for the period 1922–2005.

observed extreme indices were computed based on the daily area-averaged precipitation in each region.

c. Anomaly analysis

We utilized anomaly analysis based on model precipitation at the annual scale from the CMIP5 GCMs from the past1000 to the future2099 (Wei and Ma 2003; Huang et al. 2013). For this analysis, the averaged annual precipitation (Rmean) and averaged maximum 1-day precipitation over five regions in Europe for the period 1971–2000 from the ECA&D data were calculated as the baseline values. The deviation (%) of the annual-scale precipitation anomaly during a long-term period of 1250 years was then calculated by the percentage change of the simulated area-averaged annual precipitation (Rtot) and maximum 1-day precipitation (Rx1day) from the CMIP5 GCMs for the period 850–2099 compared with the baseline values. In addition, the 30-yr moving average method was also employed to analyze this percentage change of precipitation anomaly:

$$D_p = \frac{S_p - \overline{O_p}}{\overline{O_p}}, \tag{1}$$

where D_p, S_p, and O_p are the deviation (%) of precipitation anomaly, the simulated area-averaged precipitation indices, and the baseline value, respectively.

d. Extreme precipitation indices

According to the WMO guideline (Klein Tank et al. 2009), extreme precipitation is defined as a pronounced precipitation event occurring during a period, with daily total precipitation exceeding a certain threshold defined for a given location. In our study, the statistical analysis of extreme precipitation was based on daily precipitation and the extreme precipitation indices included the maximum 1-day, 5-day, and 15-day precipitation amounts that exceed a level associated with the chosen return periods (i.e., 5, 10, 20, 50, 100, and 200 years) for all observed stations in Europe. Moreover, the same extreme precipitation indices were applied for the five European subregions. All of the extreme precipitation indices used in this study are listed in Table 3.

In addition, we use generalized extreme value (GEV) distribution to derive the return-period-based precipitation amounts from the statistical cumulative density functions of the conceptual distributions for the precipitation extremes based on the observed data and simulated precipitation of the CMIP5 GCMs. The GEV method is widely applied for modeling extreme events in meteorology and many other fields (Coles et al. 2003; Khaliq et al. 2006). The GEV technique was introduced into meteorology by Jenkinson (1955) and is used extensively to model extreme natural phenomena such as precipitation (Gellens 2002). The probability density function (PDF) and cumulative distribution function (CDF) of the GEV are as follows:

$$f(x) = \frac{1}{\alpha}\left[1 - k\left(\frac{x-\xi}{\alpha}\right)\right]^{1/k-1} \exp\left\{-\left[1 - k\left(\frac{x-\xi}{\alpha}\right)\right]^{1/k}\right\}, \tag{2}$$

TABLE 3. Definition of extreme precipitation indices.

Acronym	Definition	Units
Rmean	Averaged annual precipitation	mm
Rtot	Area-averaged annual precipitation	mm
Rx1day	Annual maximum 1-day precipitation	mm
R50YR	Estimate of return value for 1-day, 50-yr event	mm
R100YR	Estimate of return value for 1-day, 100-yr event	mm

$$F(x) = \exp\left\{-\left[1 - k\left(\frac{x-\xi}{\alpha}\right)\right]^{1/k}\right\}, k \neq 0, \tag{3}$$

where α, ξ, and k are the scale parameter, location parameter, and shape parameter, respectively.

Estimates of the extreme quantiles, known as the return level z_p, corresponding to the return period

$$\tau = \frac{1}{p}, \tag{4}$$

where p is the probability of occurrence, can be obtained by

$$Z_p = \xi - \frac{\alpha}{k}\{1 - [-\log(1-p)]^{-k}\}. \tag{5}$$

In this study, we divided the future period 2016–99 into two 42 years including 2016–47 and 2048–99, and then we used the F test and t test (significance level 0.01) in five regions to determine whether the variance and mean of the two samples are significantly different. The results in Table 4 show that most of the areas (except for NE and EE) were stationary, so we adopted the stationary GEV assumption in the study.

e. Period division

To compare the extreme precipitation changes over the entire 1250-yr study period, we divided the time series into four equal-length periods: 959–1042 (past1), 1559–1642 (past2), 1922–2005 (history), and 2016–99 (future). This was to deal with the fact that the values of extreme precipitation indices are significantly affected by sample size (i.e., time period); thus, the time periods of extreme precipitation from various experiments should be consistent. However, the time periods of the past1000 (850–1849) and the future RCP2.6 and RCP8.5 projections (2006–99) are longer than those of the historical period and the observed ECA&D data (1922–2005). To maintain consistency, the historical period of 1922–2005 was first chosen as the evaluation period baseline due to the limited observation time span. Therefore, the same time period of 84 years in the past1000 and future projections was determined accordingly. Furthermore, in the Northern Hemisphere, during the past1000 period, paleoclimatic reconstructions were recognized to include two periods, a climatic perturbation known as the MCA and a planetary cold period referred to as the LIA, extending from 950 to 1250 and from 1500 to 1800, respectively (Matthews and Briffa 2005). Thus, we selected the periods 959–1042 within the MCA and 1559–1642 within the LIA to represent the entire past1000 projection. In addition, the RCP2.6

TABLE 4. The results of the *F* test and *t* test for the maximum 1-day precipitation under both RCP2.6 and RCP8.5 scenarios (2016–99); N means no significant difference and Y means significant difference.

Model	*F* test		*t* test	
	RCP2.6	RCP8.5	RCP2.6	RCP8.5
NE				
BCC-CSM1.1	N	N	N	Y
MIROC-ESM	N	N	N	Y
MRI-CGCM3	N	N	N	N
CCSM4	N	N	N	Y
SE				
BCC-CSM1.1	N	N	N	N
MIROC-ESM	N	N	N	Y
MRI-CGCM3	N	N	N	N
CCSM4	N	N	N	N
CE				
BCC-CSM1.1	N	N	N	N
MIROC-ESM	N	N	N	Y
MRI-CGCM3	N	N	N	N
CCSM4	N	N	N	N
EE				
BCC-CSM1.1	N	N	N	Y
MIROC-ESM	Y	Y	N	Y
MRI-CGCM3	N	Y	N	Y
CCSM4	N	N	N	Y
WE				
BCC-CSM1.1	N	N	N	Y
MIROC-ESM	N	N	N	Y
MRI-CGCM3	N	N	N	N
CCSM4	N	N	N	N

and RCP8.5 scenarios were used as the future projections (2016–99) representing anthropogenic global warming. All of the extreme precipitation indices for the observed stations and the five regions were calculated based on those four time periods.

f. Frequency distribution

One of the main questions addressed in this study was whether the last 100 years of instrumental measurements (1922–present) could adequately represent the precipitation variability and extremes statistics over a long-term period of more than 1000 years. To answer it, we analyzed the precipitation frequency distribution of Rtot and Rx1day, and their changes from the past1000 to the future2099 in five regions of Europe. Our analysis consisted of the following steps. First, the Rtot and Rx1day frequency distributions of the ECA&D observations and CMIP5 GCM simulations were obtained for the evaluation period of 1922–2005. We then compared the two simulated distributions with the observed distributions and bias-corrected the mean of the simulated Rtot and Rx1day distributions from the CMIP5 GCMs compared with the means of the observed Rtot and Rx1day distributions in the historical period. Second, the same bias corrections were applied to the Rtot and Rx1day distributions of the CMIP5 GCMs for the past1000 (past1 and past2) and the future projections. Finally, we investigated the distribution changes of Rtot and Rx1day from the historical period to the future2099 and from the past1000 (plus the historical period) to the future2099 over the five regions of Europe.

g. Statistical significant test

The *t*-test method was applied in this study to detect if the means of two data series are significantly different from each other (Efron 1969). In this test, the null hypothesis (H0) assumes that no difference exists in the mean precipitation between the two periods; the alternate hypothesis (H1) assumes difference exists in the mean precipitation between the two periods. If standardized test statistics $|T| > T_{1-\alpha/2,n+m-2}$, where n and m are lengths of the two periods, H0 is rejected and a statistically significant change exists in the hydrologic time series of two periods. The critical value of $T_{1-\alpha/2,n+m-2}$ for a significance level of 0.01 (the degree of freedom is 82) from the *t*-test critical value table is 2.637.

4. Results

a. Evaluation of precipitation in the past1000

The spatial distributions of the relative differences of seasonal precipitation between the CMIP5 GCMs and the reconstructed data are shown in Fig. 2. The CMIP5 GCMs precipitation varies more widely in the distribution compared with the reconstructed precipitation for all seasons. In general, the CMIP5 GCMs underestimate seasonal precipitation in CE, SE, the United Kingdom, and the west coast of Norway compared with the reconstructed data. Particularly in summer, all five CMIP5 GCMs underestimate the precipitation over most regions of Europe. Meanwhile, the precipitation from the CMIP5 GCMs is higher in the eastern part of NE and the northern part of CE than the reconstructed precipitation for all seasons except summer. In addition, the spatial distributions from the five CMIP5 GCMs are similar, although differences exist in various regions.

b. Evaluation of precipitation in the historical period

The differences between the CMIP5 GCMs and the ECA&D from 1922 to 2005 for Rmean, Rx1day, and estimates of return values for 1-day, 100-yr events (R100YR) are depicted in Fig. 3. When comparing the model-simulated precipitation climate with observations, it can be seen that in general the CMIP5 GCMs tend to overestimate the Rmean values in almost all areas of NE, CE, and WE while underestimating Rmean in some areas of SE and EE. However, the CMIP5 GCMs underestimate Rx1day and R100YR in Europe even while Rmean is overestimated in some regions, although differences about the over- or underestimation level can be seen from different GCM models. For example, in NE, a bias of Rmean is up to about +200% from CCSM4 while whose biases of Rx1day and R100YR are still from around −20% to −40%. This indicates that the CMIP5 GCMs tend to underestimate the magnitude of extreme precipitation events over most regions of Europe, as shown in Figs. 3b and 3c.

Boxplots of the bias from the CMIP5 GCMs compared with the ECA&D data for four precipitation indices—Rmean, Rx1day, and estimates of return value for 1-day, 50-yr events

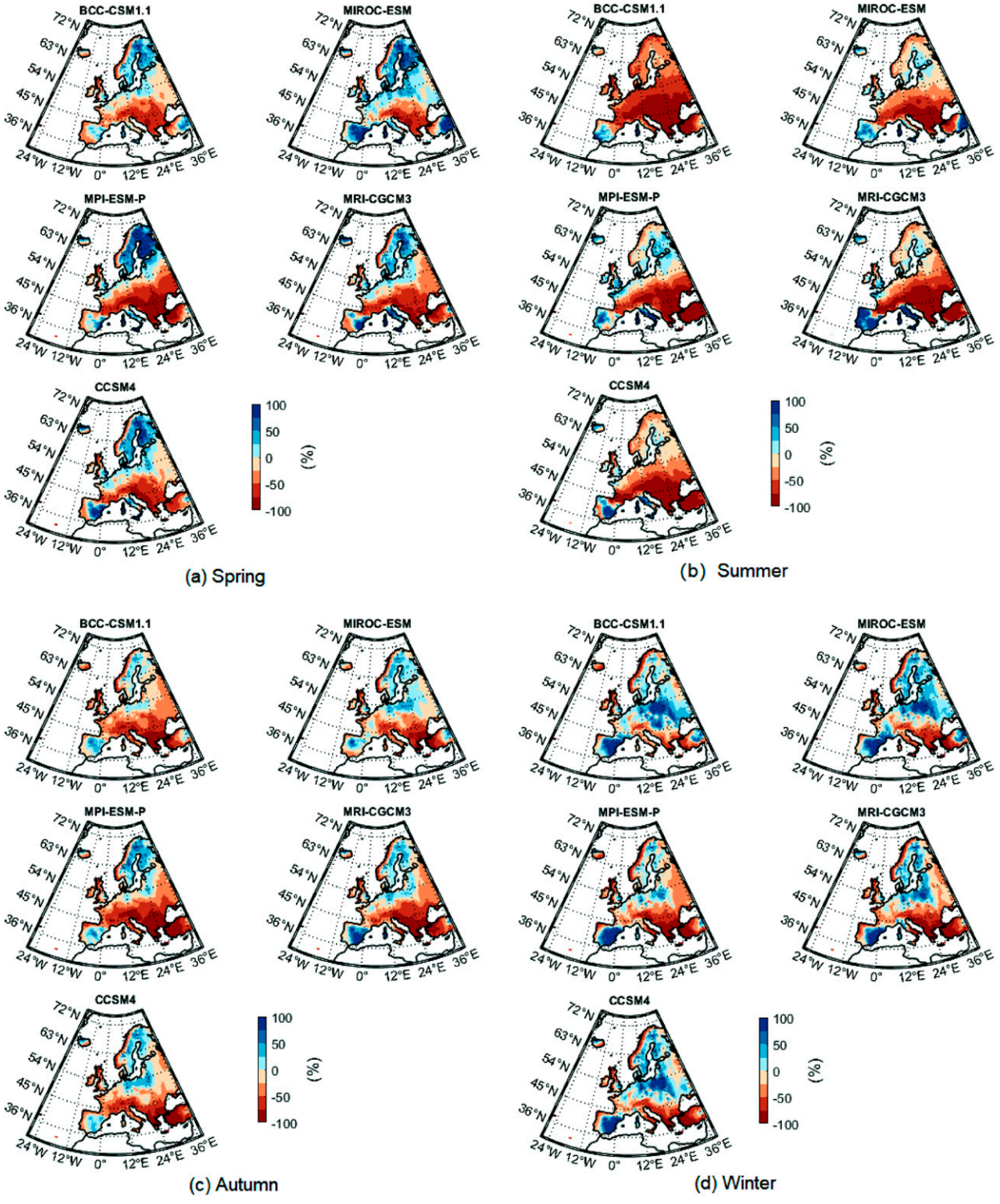

FIG. 2. Spatial distributions of the relative precipitation differences between the five GCMs and the reconstructed data (1500–1850) in (a) spring, (b) summer, (c) autumn, and (d) winter.

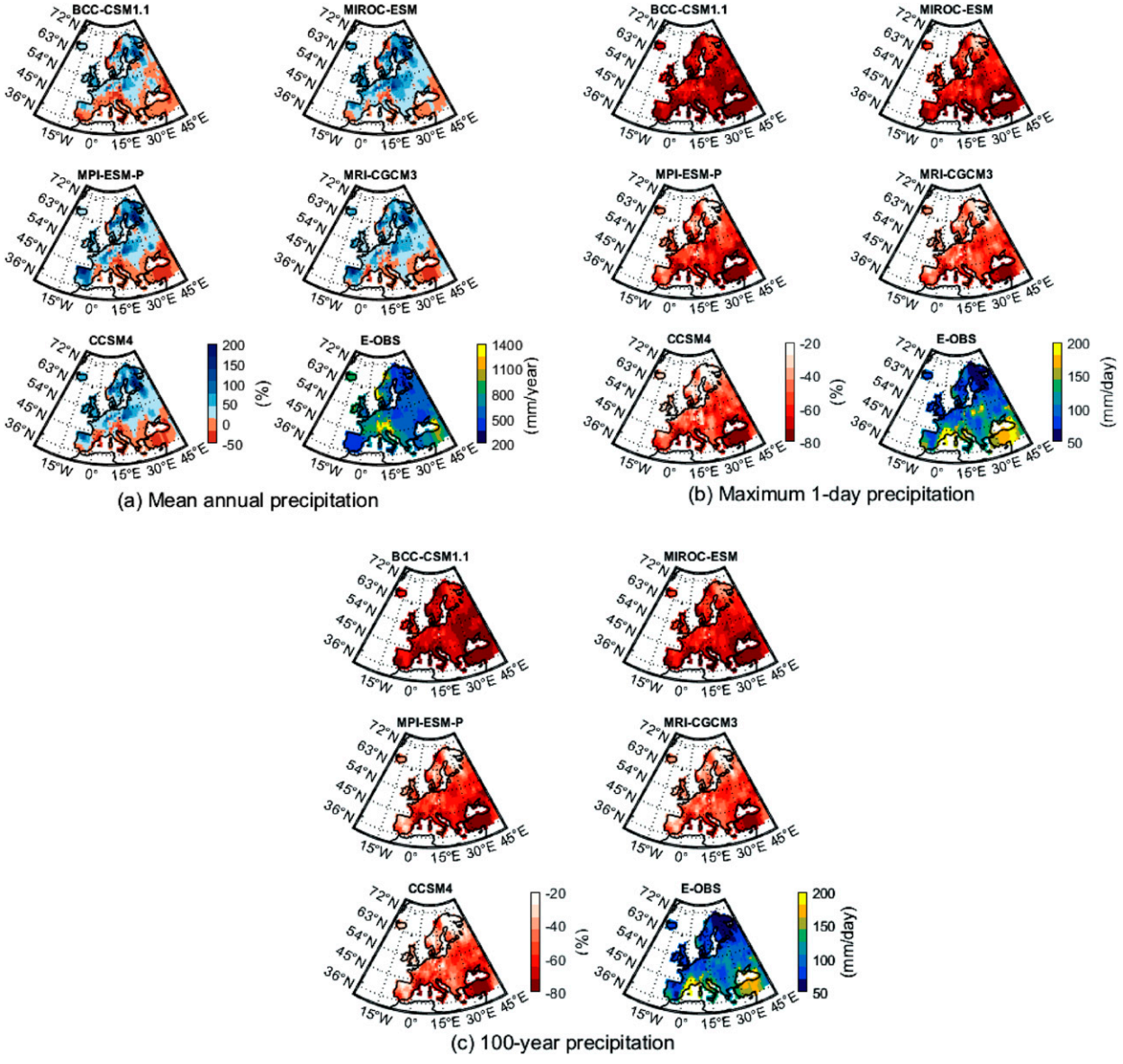

FIG. 3. Spatial distributions of the relative precipitation differences between the CMIP5 GCMs and ECA&D observations for the period 1922–2005 for (a) mean annual precipitation, (b) maximum 1-day precipitation, and (c) estimates of return values for 1-day, 100-yr events. The relative differences are equal to model simulations minus observations, divided by observations.

(R50YR) and R100YR—in the five European regions are plotted in Fig. 4. It can be seen that almost all regions exhibit positive biases of Rmean and negative biases of the other three extreme indices (Rx1day, R50YR, and R100YR). Only the CCSM4 model shows a negative value of the median for Rmean in SE although there is a clear positive skewness to the upper quartile. That is to say, the CCSM4 Rmean is slightly underestimated in some areas of SE compared with the ECA&D. These results are consistent with the findings depicted in Fig. 3. In addition, from Fig. 4, we can also see that some models display poor skill in the simulation of extreme precipitation while providing good estimates of Rmean. For example, although the box plots of the Rmean biases from the BCC-CSM1.1 model show narrower ranges and better medians, which are closer to 0 compared with other models, this model performs poorly in these five regions when simulating extreme indices. Koutroulis et al. (2016) investigated the overall agreement between the probability density functions, derived from daily precipitation or different percentile values, of the observed and the 23 GCMs' data. They found that same GCM shows distinct abilities for simulating the distribution of mean and extreme precipitation, which was consistent with the results in our study.

Figure 5 shows the empirical distributions of Rtot and Rx1day from the CMIP5 GCMs over all five regions in the

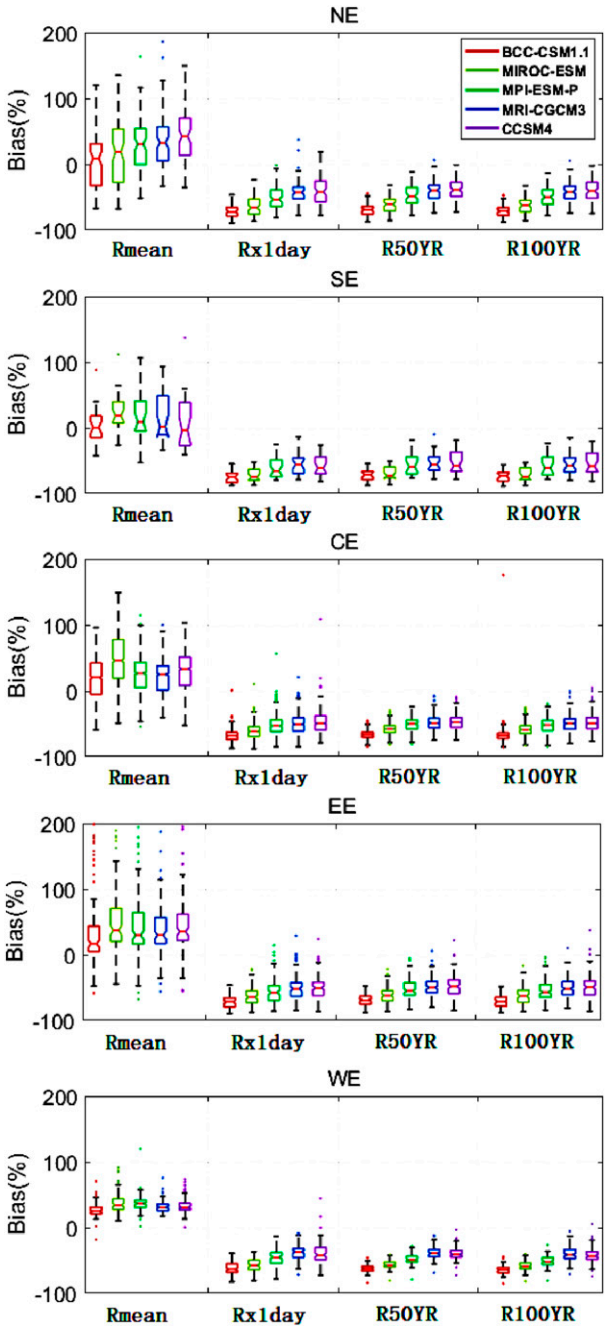

FIG. 4. Boxplots of distributions of the biases between the CMIP5 GCMs and ECA&D station data of the four indices from 1922 to 2005 for all five European regions—Rmean: averaged annual precipitation, Rx1day: maximum 1-day precipitation, R50YR: estimate of return value for 1-day, 50-yr event, and R100YR: estimate of return value for 1-day, 100-yr event.

historical period compared with those from the observations. The distributions of Rtot and Rx1day from the CMIP5 GCMs vary considerably, and the intraregional differences are almost as large. In general, the Rtot values from almost all CMIP5 GCMs are higher than the observed values with the same value of $F(x)$ in all regions except BCC-CSM1.1 and MIROC-ESM models of NE. All of the CMIP5 GCMs underestimate the Rx1day magnitude in CE and SE. What is interesting is that the BCC-CSM1.1 and MIROC-ESM models underestimate the Rx1day magnitude in other three regions, but other models (i.e., MPI-ESM-P, MRI-CGCM3, and CCSM4) overestimate the Rx1day magnitude compared with observed Rx1day. The distribution patterns of Rtot from the CMIP5 GCMs display no clear consistency with those from observations. In addition, the Rx1day distributions from the MRI-CGCM3 and CCSM4 models are the most consistent with those from the ECA&D observations in NE, EE, and WE.

c. *Anomaly analysis*

The area-averaged time series of annual precipitation anomalies (in percent) over 1250 years including past1000 (850–1849), historical (1850–2005), and future (2006–99) projections in the five European regions are presented in Fig. 6. Figure 7 shows a similar presentation of the maximum 1-day precipitation anomalies. For both Figs. 6 and 7, the baseline values are the observed precipitation for 1971–2000 from the ECA&D, as shown in Eq. (1). The inconsistency of 1850 between the two periods of past1000 (850–1849) and historical (1850–2005) is smoothed by 30-yr moving averaging in Figs. 6 and 7. We can see from the figures that 1) compared with the observed precipitation, the annual precipitation values (Rtot) from the CMIP5 GCMs are overestimated, while the extreme precipitation values (Rx1day) from these models are underestimated; 2) there is a stable fluctuation of Rtot before 1950 and an obvious increase after 1950 until the end of the twenty-first century under both two RCP scenarios across all of Europe, with the exception of SE; 3) obvious increases are exhibited in all CMIP5 GCMs simulations of Rx1day after 1950 until the end of the twenty-first century under both two RCP scenarios across all of Europe; and 4) the uncertainty bands of the future Rtot and Rx1day increase are wide regarding both scenarios. The Rtot and Rx1day values are projected to increase much more from the RCP8.5 scenario than that from the RCP2.6. Additionally, 5) the MIROC-ESM model displays the highest future increases from the RCP 8.5 for both Rtot and Rx1day compared with the other CMIP5 GCMs, although all of the CMIP5 GCMs project increase; and 6) it should be noted that over SE, the increase of extreme precipitation is associated with a decrease in annual precipitation. This inconsistency may be a result of an increased number of dry days in combination with more intense convective extremes, translating to lower mean precipitation, which may result in more hazards from both floods and droughts (Fowler et al. 2007).

d. *Spatial distribution changes*

The changes of spatial distribution of Rmean and average Rx1day of the CMIP5 GCMs from past1 to past2, from past2 to the historical period, and from the historical period to the future2099 are illustrated in Figs. 8 and 9. The grid points of Rmean and average Rx1day with nonsignificant change at the 0.01 significance level based on the t test are shown. As shown in Fig. 8a, the range of Rmean changes from past1 to past2 varies from −5% to 5% in most areas and Rmean values tend

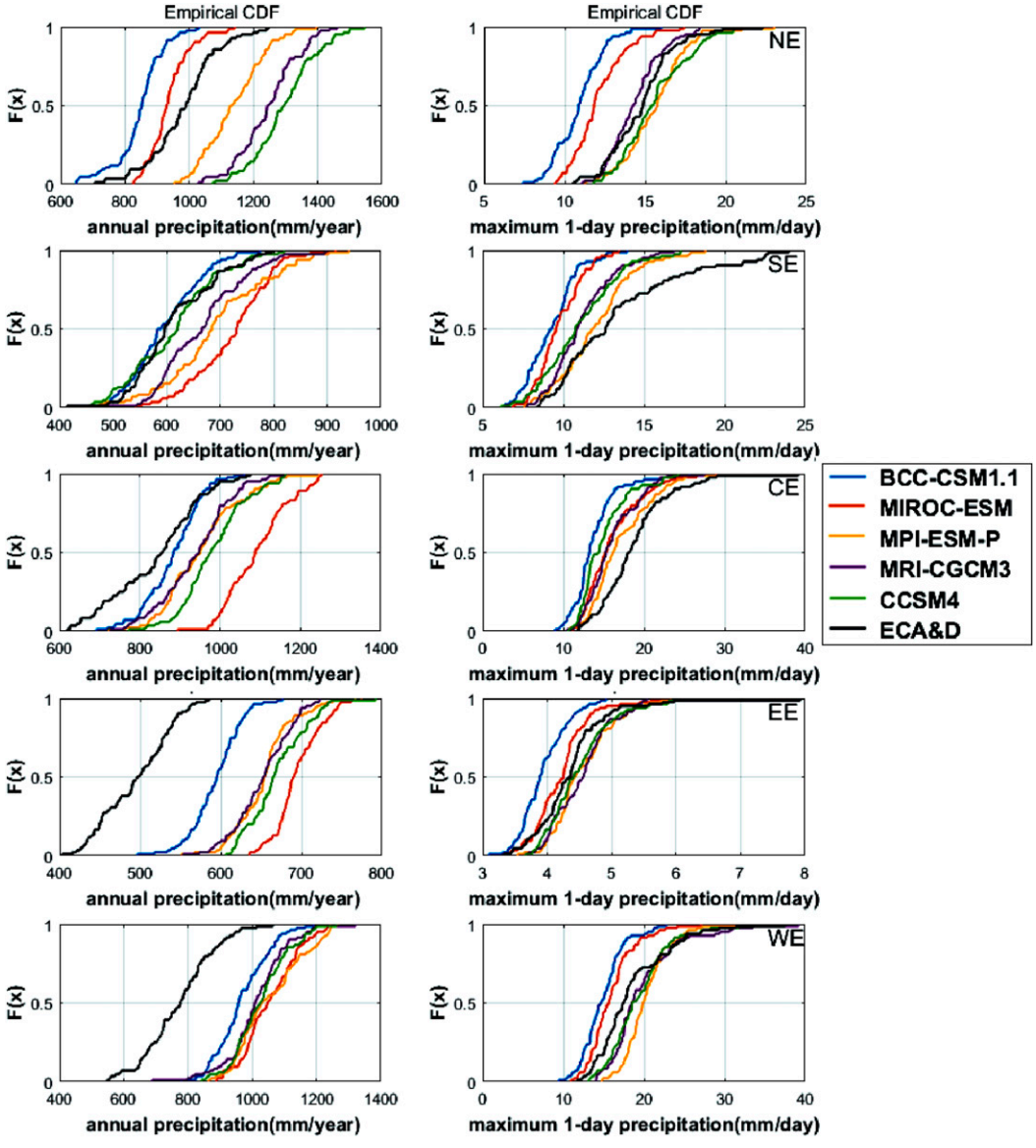

FIG. 5. The empirical distributions of annual precipitation and maximum 1-day precipitation during the historical period (1922–2005) in each of the five European regions for the five CMIP5 GCMs. The *x* axis is the calculated Rtot and Rx1day values, and the *y* axis is the value of empirical distribution function.

to increase in some areas of NE and decrease in most areas of southwestern Europe from past1 to past2. In addition, the differences between models are relatively large. For example, there is an obvious decrease in WE, SE, CE, and EE for MPI-ESM-P and MRI-CGCM3; conversely, MIROC-ESM shows an increase in the same regions except Spain and Portugal. Figure 8b reveals that the range of Rmean changes from past2 to historical, varying from −10% to 10%, is larger than that from past1 to past2. Moreover, there is an increase in NE and a decrease in SE, CE and most areas of EE for BCC-CSM1.1, MRI-CGCM3, and CCSM4, but MPI-ESM-P and MIROC-ESM indicate a decreasing trend over almost the whole of Europe. We can also see that almost all GCMs show no significant change in mean annual precipitation from past1000, including both the past1 (959–1042) and past2 (1559–1642) periods, to the historical period for the vast majority of grid points in Figs. 8a and 8b, except MPI-ESM-P from past2 to historical. There are no grid points or only a few grid points with significant change from the ensemble mean of all GCMs. This may because only a few grid points show significant change and the uncertainty of limited models. In general, Figs. 8a and 8b illustrate that there are minor changes from the past1000 (including past1 and past2) to the historical period.

Larger changes varying from −20% to 20% from the historical period to the future2099 under both the RCP2.6 and RCP8.5 scenarios than that from the past1000 to the historical

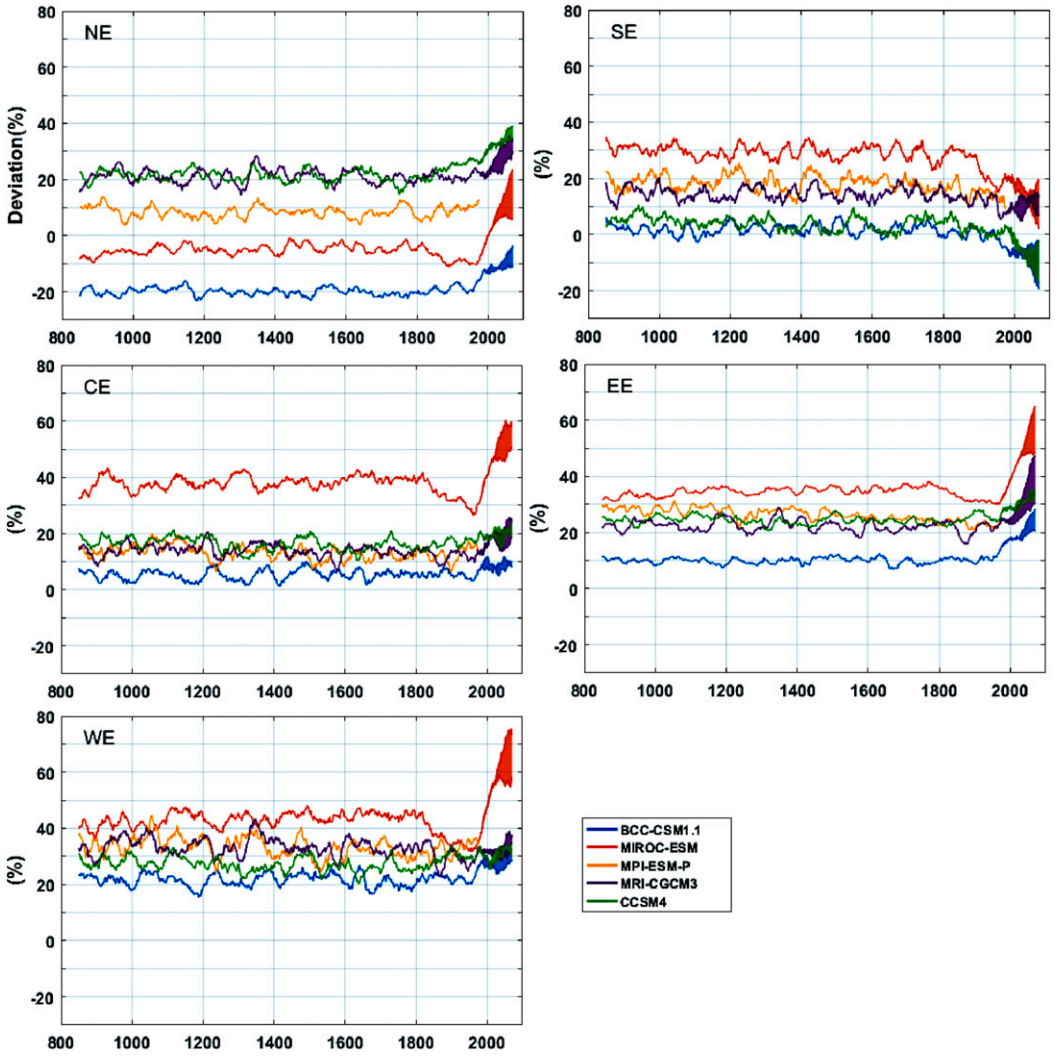

FIG. 6. The 30-yr moving average of the percentage of areal-averaged annual precipitation anomalies from the past1000 to the future2099 (RCP2.6 and RCP8.5) for each model and region. The lower and upper bounds of the uncertainty bands of future period represent the RCP2.6 and RCP8.5 scenario, respectively.

period are shown in Figs. 8c and 8d. In addition, Rmean tends to increase in most areas in the future, with the exception of some decreases in SE, especially in Spain and Portugal with a decrease, confirming the results shown in Fig. 6. Also, there are more areas exhibiting significant changes for almost all GCMs from the historical period to the future2099, especially a significant increase in NE.

For the average Rx1day extreme precipitation indices shown in Figs. 9a and 9b, we can see that the changes from past1 to past2 and from past2 to the historical period from all CMIP5 GCMs display similar spatial distributions to Rmean, which is helpful to discern uniform trend for a particular region. In addition, only a very small percentage of grid points show a statistical difference for average Rx1day from past1 to past2 and from past2 to the historical period for all GCMs. Moreover, the average Rx1day changes varying from −20% to 20% over some areas of Europe from the past1000 to the historical period are greater than the range of Rmean changes.

All of the CMIP5 GCMs indicate that Rx1day will most likely increase across most of Europe from the historical period to the future2099 under both the RCP2.6 and RCP8.5 scenarios in Figs. 9c and 9d. Additionally, the changes of Rx1day from the historical period to the future2099 are projected to reach 30% in many areas under the RCP8.5 scenario. In Fig. 9d, we could see that in general, the maximum 1-day precipitation increases from historical to RCP8.5 in most grid points of Europe. The increases in most of the grid points are statistically significant from all GCMs except CCSM4 and from the ensemble mean result. It is worth noting that the increase of the maximum 1-day precipitation from historical to future2099 under the RCP2.6 scenario is less than that under the RCP8.5 scenario.

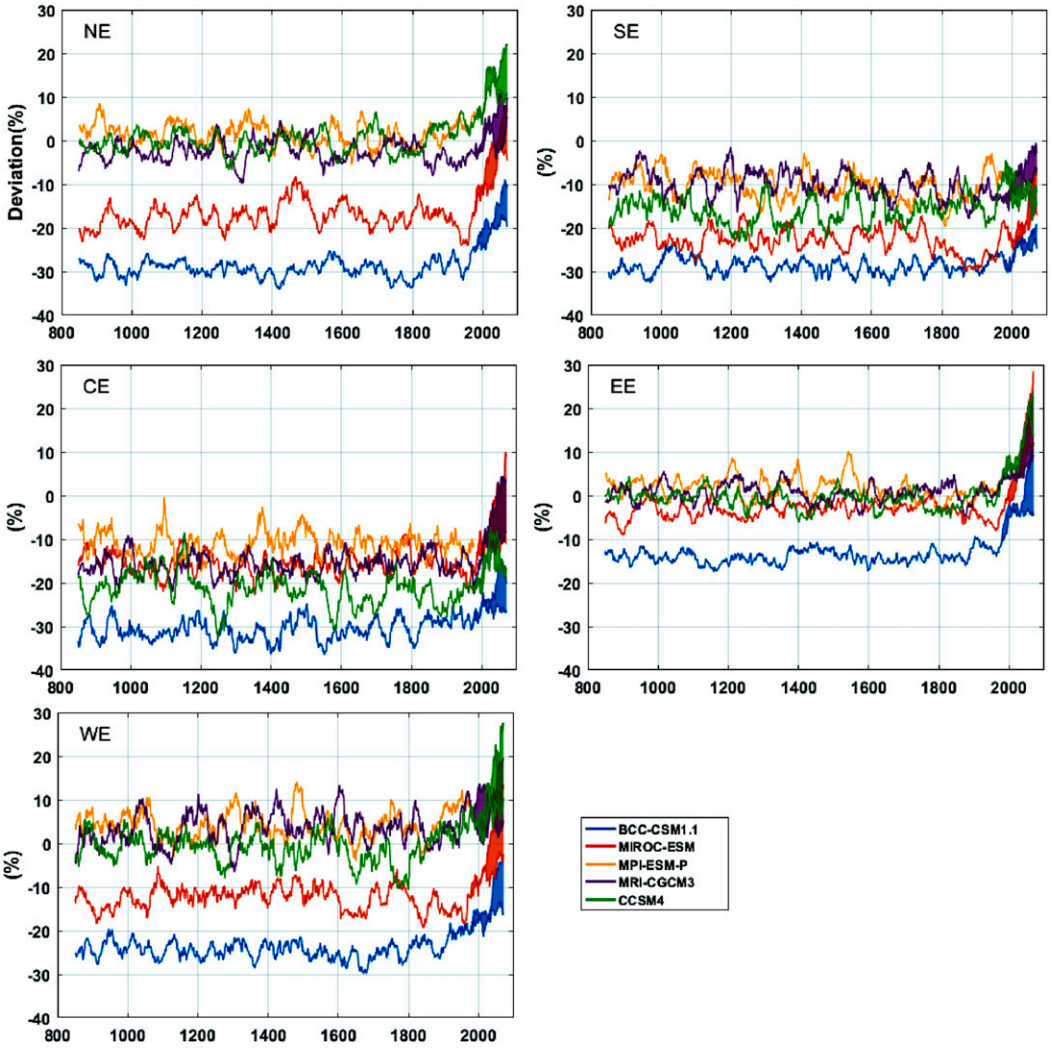

FIG. 7. The 30-yr moving average of the percentage of areal-averaged maximum 1-day precipitation anomalies from the past1000 to the future2099 (RCP2.6 and RCP8.5) for each model and region. The lower and upper bounds of the uncertainty bands represent the RCP2.6 and RCP8.5 scenario, respectively.

In addition, a comparison of the geographical patterns of changes in Rmean and Rx1day reveals that the projected Rmean and Rx1day increases coincide in some areas. In those areas (e.g., NE), more extreme precipitation events are projected to occur. To conclude, Figs. 9 and 10 reveal that there are no big changes of extreme precipitation from the past1000 to the historical period, while an obvious increasing trend of extreme precipitation from the historical period to the future2099 is seen.

e. Extreme indices changes

Figures 10 and 11 show the estimated 1-, 5-, and 15-day precipitation from the ensemble mean of five CMIP5 GCMs under 5-, 10-, 20-, 50-, 100-, and 200-yr return periods from the past1000 to the future2099.

In general, the ensemble mean of five CMIP5 GCMs shows no robust change trend from the past (past1 and past2) to the historical period for 1-, 5-, and 15-day precipitation amounts under different return periods in Europe. By contrast, it is clear that the extremes in the future are predicted to increase in the context of climate change. There are, however, some exceptions, such as the fact that the future 1- and 5-day precipitation amounts for 100- and 200-yr return periods of the model ensemble mean under the RCP2.6 scenario are less than the historical period values in CE. In some regions of CE, Rx1day is projected to decrease, which may mean a decrease in extreme events. In general, the precipitation extreme events under the RCP8.5 scenario are projected to increase much more than that from the RCP2.6 scenario for most CMIP5 GCMs and regions.

In addition, as the return period gets longer, the extremes projected by the RCP8.5 show a greater increase in magnitude, especially for the 100-yr precipitation and 200-yr precipitation. There is an overall decreasing trend in return periods for each

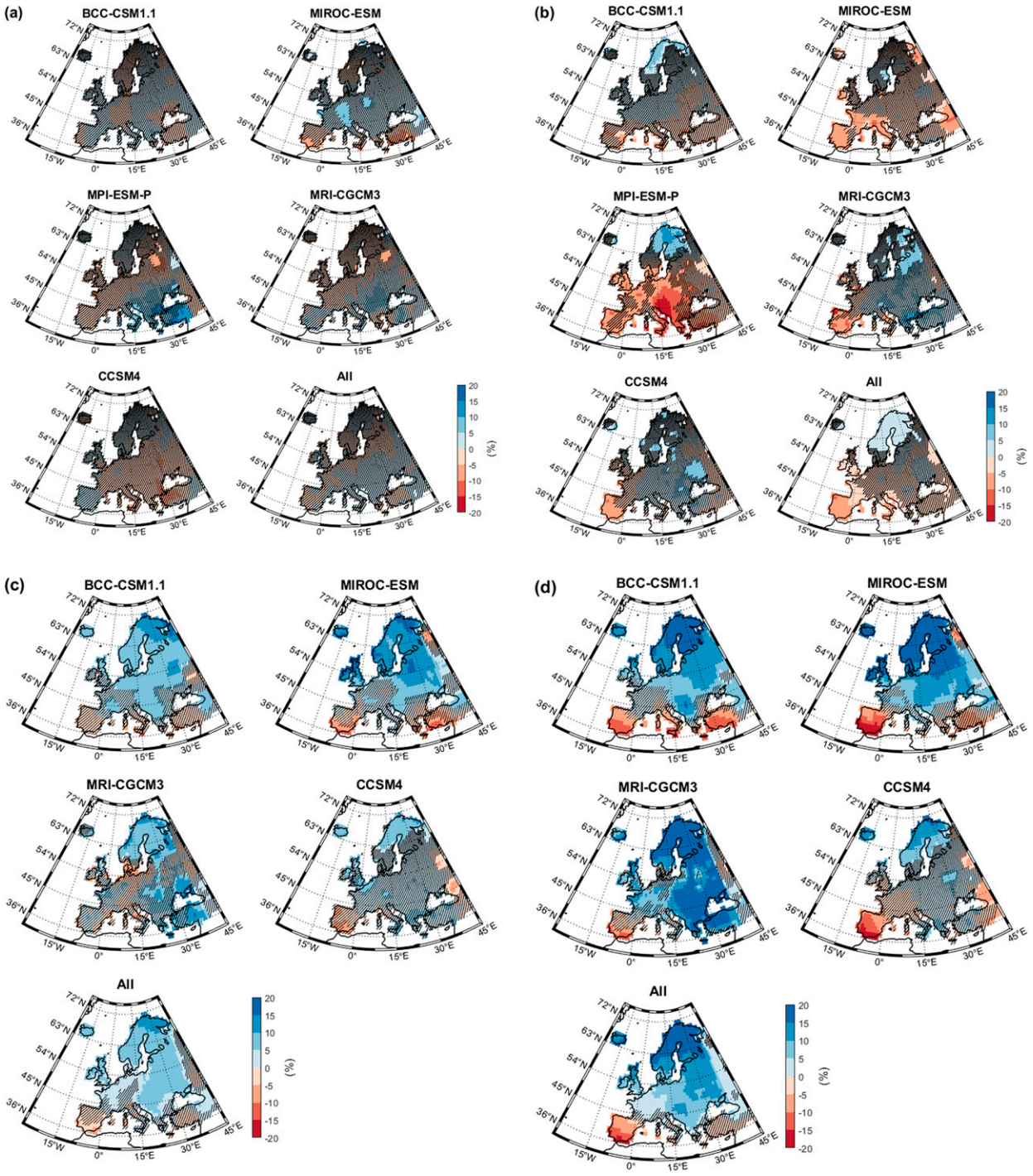

FIG. 8. Relative changes in the average annual precipitation across Europe during the periods (a) from past1 to past2, (b) from past2 to historical, (c) from historical to RCP2.6, and (d) from historical to RCP8.5. In all cases, the relative changes are computed by dividing the differences of average annual precipitation between the two periods by the corresponding value of the previous period. The oblique line denotes nonsignificant change at the 0.01 significance level based on the *t* test. The subgraph titled ''All'' shows the changes in ensemble mean of five GCMs.

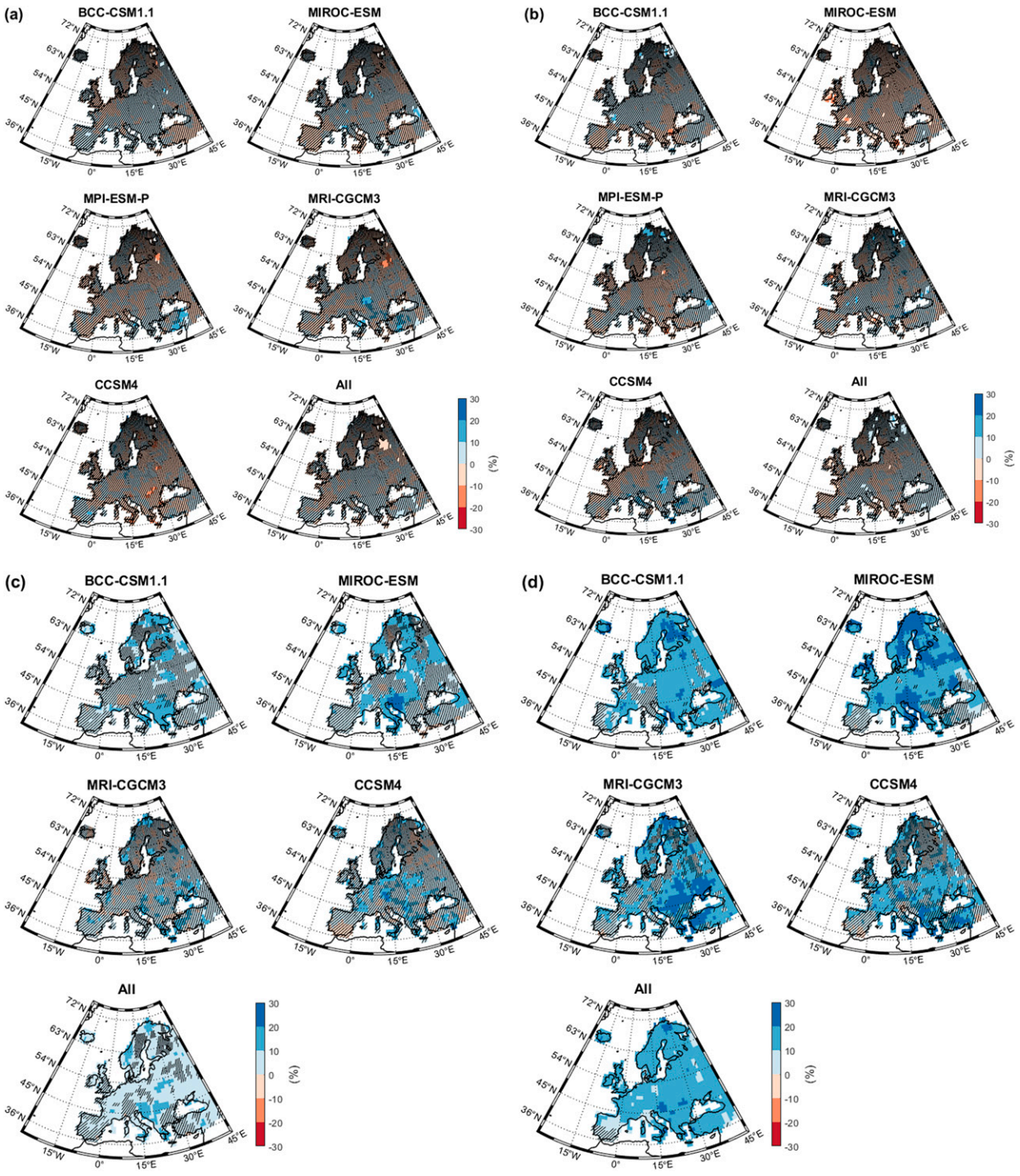

FIG. 9. Relative changes in the average maximum 1-day precipitation across Europe during the periods (a) from past1 to past2, (b) from past2 to historical, (c) from historical to RCP2.6, and (d) from historical to RCP8.5. In all cases, the relative changes are computed by dividing the differences of average maximum 1-day precipitation between the two periods by the corresponding value of the previous period. The oblique line denotes nonsignificant change at the 0.01 significance level based on the *t* test. The subgraph titled "All" shows the changes in ensemble mean of five GCMs.

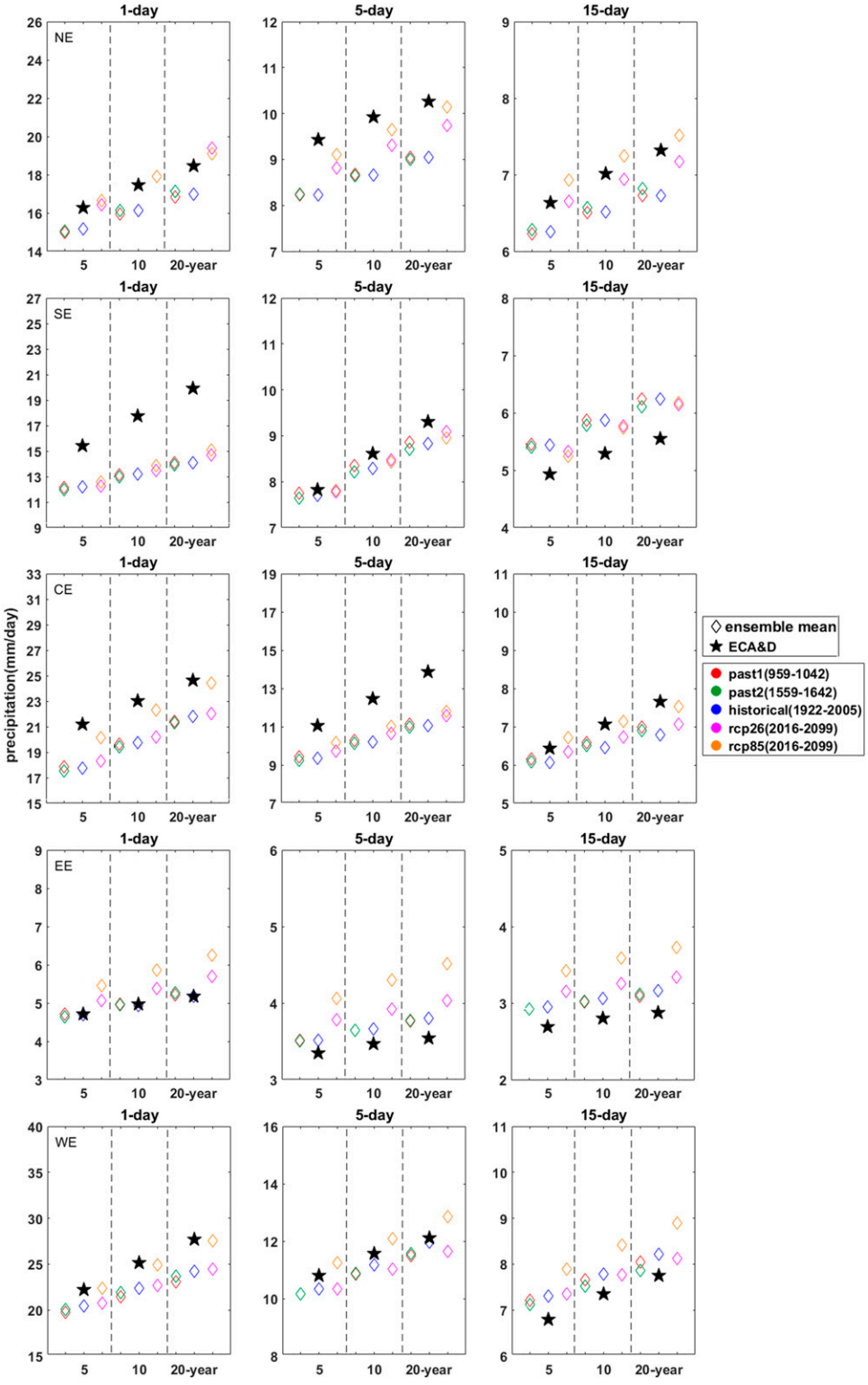

FIG. 10. Changes of extreme indices (1-, 5-, and 15-day precipitation) with different return periods (5, 10, and 20 yr) from past1000 to future2099.

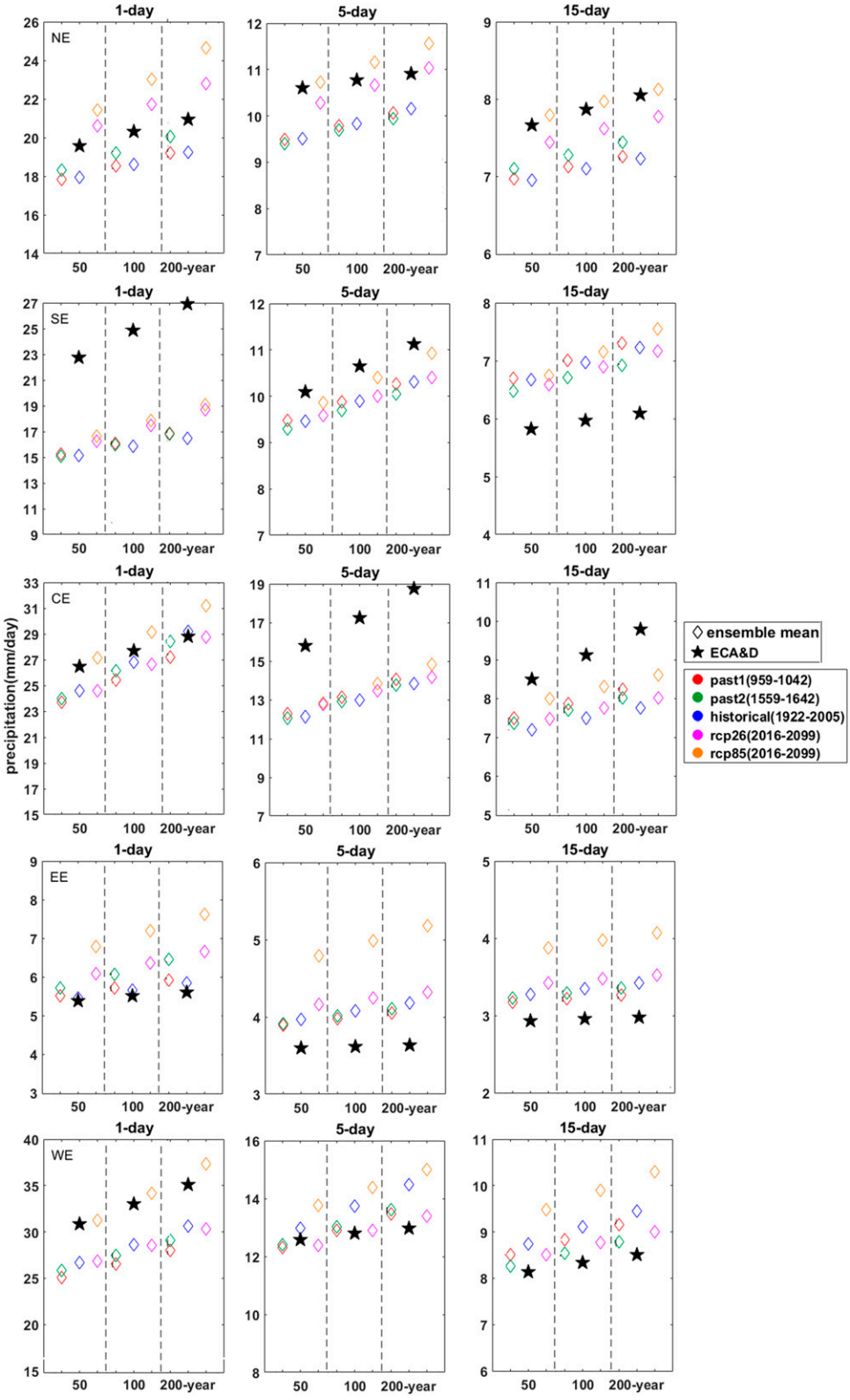

FIG. 11. Changes of extreme indices (1-, 5-, and 15-day precipitation) with different return periods (50, 100, and 200 yr) from past1000 to future2099.

extreme index that is indicative of increasing precipitation extremes. The 1-day, 200-yr return period values of the model ensemble mean in CE in the historical period become approximate or even less than 100-yr return events in the future for the RCP8.5, which is also similar to other extreme indices. From Figs. 10 and 11, we can also see that short-duration extreme precipitation such as 1-day precipitation under different return periods will increase significantly. This result indicates that the greater the number of consecutive days, the smaller the precipitation change from the years 850–2099, regardless of the return period.

f. Extreme frequency distribution changes

Figure 12 shows the frequency distribution changes of Rtot in all regions of Europe: from the past1 to the past2; from the past2 to the historical period; from the historical period (1922–2005) to the future (2016–99); and from the past1000 [i.e., 959–1042 (past1) and 1559–1642 (past2)] plus the historical period to the future2099. From these results, we can see that the frequency of higher Rtot is projected to increase in the future from both two emission scenarios compared with that from the historical period for all CMIP5 GCMs in all of Europe except SE. For example, in the future, values of Rtot varying from 800 to 1000 mm yr^{-1} drop in frequency while the frequency of values varying from 1000 to 1500 mm yr^{-1} increases in both the RCP2.6 and RCP8.5 scenarios for all CMIP5 GCMs in NE. An opposite change can be seen in SE, with the Rtot projected to decrease from 500–700 to 300–400 mm yr^{-1}, which confirms the results in Figs. 6, 8c, and 8d. A wider range of changes of frequency distribution can be found in the future from the RCP8.5 scenario compared with that from the RCP2.6 scenario for most of the CMIP5 GCMs. Also, when comparing the changes from the historical period to the future2099 and the changes from the past1000 (plus the historical period) to the future2099, the difference varies more in the CMIP5 GCMs than in regions. For example, the BCC-CSM1.1 and CCSM4 models have the same waveforms, while the waveforms of the other two models, MIROC-ESM and MRI-CGCM3, are the opposite, which indicates that frequency changes of the Rtot from the past1000 to the historical period from four CMIP5 GCMs are of large uncertainty. Finally, the changes of frequency distribution from the past1 to the past2 (first column) and from the past2 to the historical period (second column) vary from −20% to 20% except MIROC-ESM, which also indicates minor changes of Rtot from past1000 to the historical period.

Similar to Fig. 12, Fig. 13 shows the frequency distribution changes of Rx1day in all regions of Europe: from the past1 to the past2 periods; from the past2 to the historical period; from the historical period (1922–2005) to the future (2016–99), and from the past1000 [i.e., 959–1042 (past1) and 1559–1642 (past2)] plus the historical period to the future2099. We can see from Fig. 13 that the frequency of higher Rx1day values is projected to increase significantly in the future from both two emission scenarios compared with that from the historical period; for example, there is an increase in the frequency of Rx1day with 15–25 mm and a decrease in the frequency of Rx1day with 5–15 mm for the BCC-CSM1.1 and MIROC-ESM in NE under both the RCP2.6 and RCP8.5 scenarios. The increase of Rx1day in the future can be found in all CMIP5 GCMs in Europe but magnitude varies in the different regions and different CMIP5 GCMs, especially in EE, where the change is miniscule. Also, the changes of frequency distribution in Rx1day from past1 to past2 (first column) and from past2 to the historical period (second column) vary from −10% to 10% for almost all CMIP5 GCMs, showing that precipitation extremes change very little from past1000 to the historical period. Finally, there are small differences of frequency change between the third and fourth column in all regions, which indicates that with or without the past1000, the distribution changes of Rx1day from the historical period to the future2099 are quite similar.

Overall, there are no consistent impacts but small changes from all CMIP5 GCMs can be seen about the magnitude and frequency change of Rtot and Rx1day from the past1000 to the historical period. However, there is a significant increase in the magnitude and frequency of extreme precipitation projections from the past1000/historical period to the future2099, which indicates a potential nonstationary characteristic of European precipitation extremes under warming climate.

5. Discussion

a. Comparison of the changes between the mean and extreme of the precipitation

When comparing the CMIP5 GCM-simulated precipitation with observations, it can be found from above results that the mean precipitation is evidently overestimated in most regions of Europe and underestimated in some areas of southern and eastern Europe, while CMIP5 GCMs tend to underestimate the precipitation extremes (e.g., maximum 1-day precipitation and 100-yr precipitation). Similar results can be found in previous studies in Europe. For example, Lehtonen et al. (2014) found that GCMs tend to underestimate the frequency and intensity of heavy precipitation events, while RCMs with their finer horizontal resolution performed well in simulating extreme precipitation. Chan et al. (2014a,b) and Kendon et al. (2014) also compared the errors and differences in the precipitation simulated by the same RCMs at two different spatial resolutions (i.e., 1.5 and 12 km). They concluded that the convection-permitting RCM (at 1.5 km) is more suitable to represent extreme precipitation than the RCM at lower spatial resolution, which underestimates daily extremes. Therefore, the coarse resolution of GCMs may not be enough to describe convective precipitation and orographic precipitation, which is probably one of the main reasons for the underestimation of extreme precipitation in GCMs.

The percent changes in precipitation extremes are not entirely correlated with the changes in mean precipitation among GCMs projections in this study. It can be found that annual precipitation is projected to decrease over southern Europe and increase in other regions, but precipitation extremes are projected to increase over most of Europe. This is consistent with the results of Trenberth et al. (2007), who concluded that the number of heavy precipitation events (e.g., the 95th percentile) increased across many land areas, even in regions with a reduction in total precipitation amounts. In most regions of Europe, increases in extremes are likely to be related to

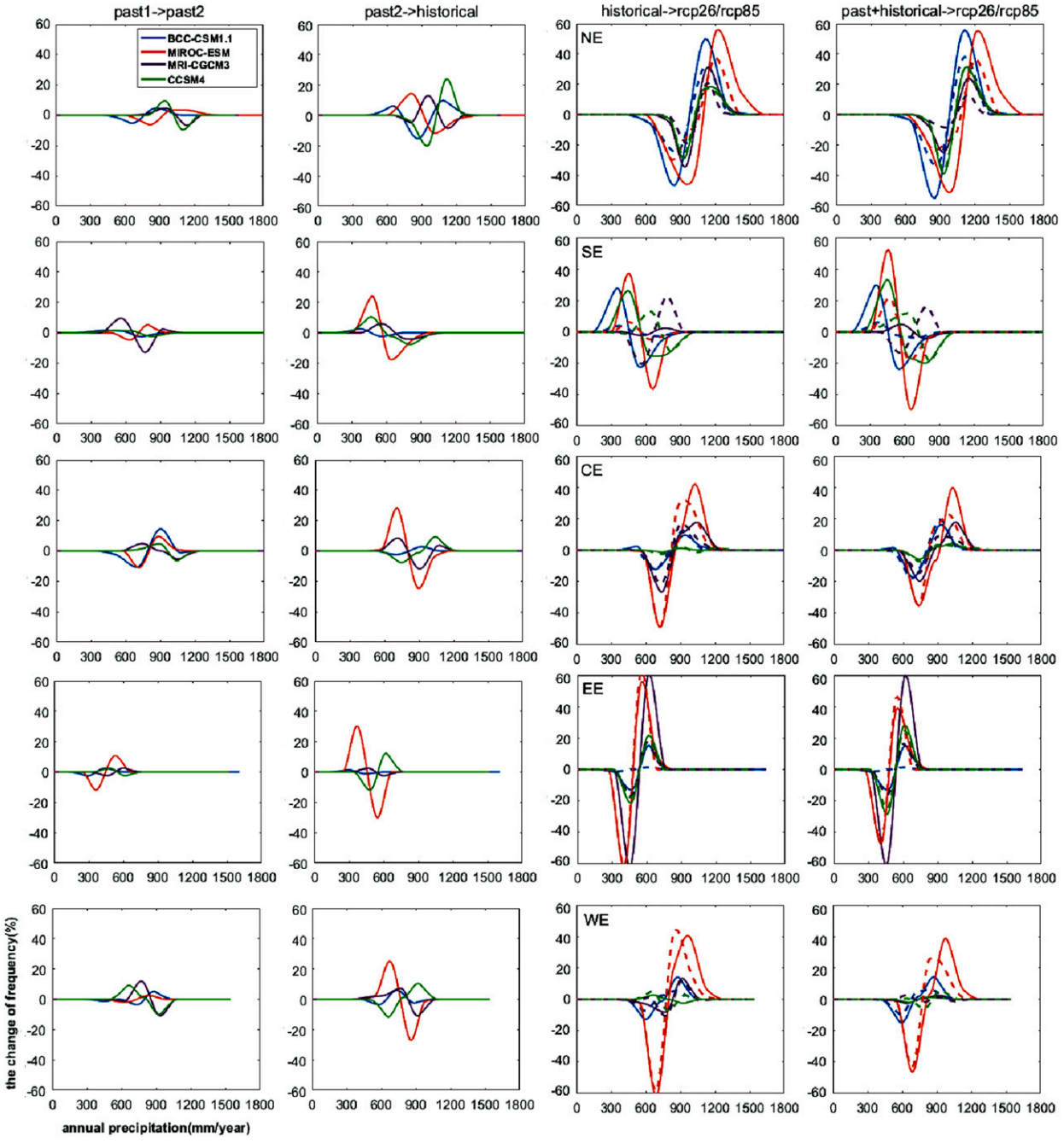

FIG. 12. Absolute changes of annual precipitation frequency in each region (first column) from past1 to past2, (second column) from past2 to the historical period, (third column) from the historical period to future2099, and (fourth column) from past1000 to future2099. Dotted lines represent the RCP2.6 scenario, and solid lines represent the RCP8.5 scenario.

proportionately more precipitation in areas affected by existing storm tracks and associated dynamical moisture convergence, which lead to the greater moisture-holding capacity of warmer air in combination with a slight poleward shift of the midlatitude storm tracks (Lehtonen et al. 2014). However, in parts of southern Europe, increases in precipitation extremes are associated with decreases in annual precipitation. This inconsistency may be a result of an increased number of dry days together with more intense convective extremes, resulting in lower annual precipitation.

b. *Projected changes in European extreme precipitation indices*

On the European scale, both short-duration and longer return-period extreme precipitation events are projected to increase considerably except in southern Europe in the future

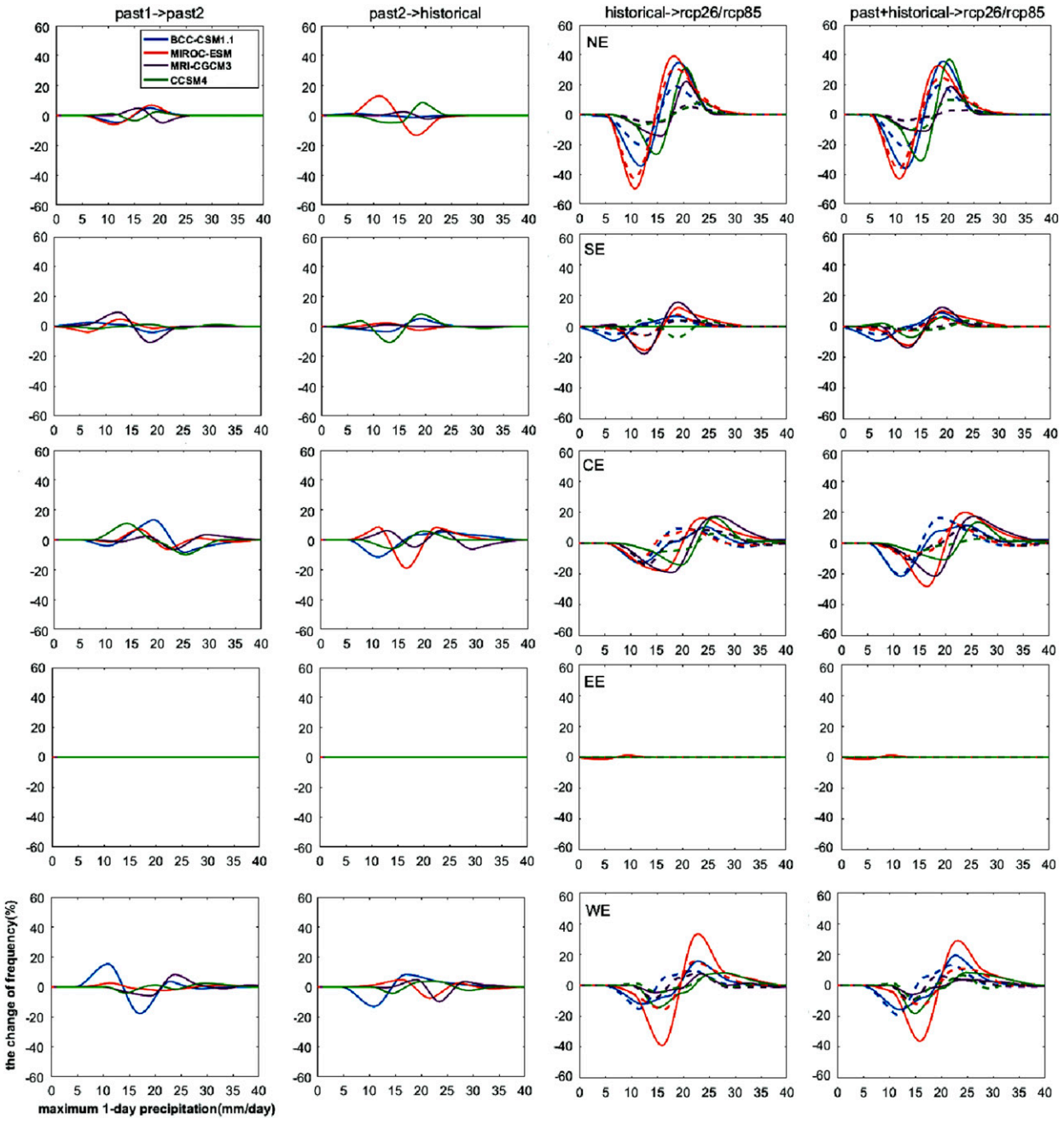

FIG. 13. Absolute changes of maximum 1-day precipitation frequency in each region (first column) from past1 to past2, (second column) from past2 to the historical period, (third column) from the historical period to future2099, and (fourth column) from past1000 to future2099. Dotted lines represent the RCP2.6 scenario, and solid lines represent the RCP8.5 scenario.

(2006–99) in this study, although there is uncertainty as to the absolute magnitude. Christensen et al. (2019) also pointed out while projections using large ensembles of GCMs consistently indicate a future decrease in summer precipitation over southern Europe [confirming the results of Barcikowska et al. (2020)] and an obvious increase over northern Europe, individual models substantially modulate these distinct signals of precipitation changes. Also, Hodnebrog et al. (2019) found that daily and subdaily extreme precipitations intensify compared to the mean in most of the European regions for a wide range of GCMs and RCMs. The increase of heavy precipitation events is also consistent with the theory of a warming climate (Prein et al. 2017; Allen and Ingram 2002) and the observed significant increasing amounts of water vapor in the atmosphere (Lenderink and Fowler 2017; Willett et al. 2008). In addition, several other climate variables in the future exhibit a

tendency toward wetter conditions. For example, 1000-hPa relative humidity and cloudiness in wintertime showed increasing trends at high latitudes (Ruosteenoja et al. 2017), which could also contribute to the increase of extreme precipitation.

We acknowledge that there will be uncertainty in the extreme precipitation analysis using stationary GEV for future RCP8.5. However, it will not impact the main conclusions of our study since the main goal of our work is not to examine how much extreme precipitation increase in the future under RCP8.5. The return period of precipitation extreme events in historical periods will become smaller in the future. For example, 200-yr events in the historical period will likely occur more often (i.e., becoming 100-yr events) in the future under the RCP8.5 scenario for almost all regions of Europe. The differences of the precipitation extremes change between the historical and future periods are in line with some existing studies of Europe. For annual 5-day and 10-day precipitation amounts in the United Kingdom, Fowler and Kilsby (2003) found that 50-yr events for the period 1961–90 became 8-, 11-, and 25-yr events in eastern, southern, and northern Scotland during the 1990s. More recently, Martel et al. (2020) suggested that extreme precipitation (i.e., a 100-yr return period over the reference period) becomes 2 to 4 times more frequent for maximum 1-day and 5-day precipitation in Europe in the future.

c. *European extremes in longer time from the past1000 to the historical period*

This study has explored the characteristics of precipitation extremes in Europe from past1000 to future2099. We find that all CMIP5 GCMs show a mild variability based on statistical significance test in extreme precipitation changes from past1 (the subperiod in the MCA) to past2 (the subperiod in the LIA). In addition, changes in the magnitude and frequency of precipitation extremes from the past1000 to the historical period are not clear and consistent with each other among the CMIP5 GCMs. However, an increase of precipitation extremes is detected to be unambiguously and statistically significant in anthropogenically forced simulations from the nineteenth century to the end of the twenty-first century, which is confirmed with previous studies (Fowler et al. 2007; Lehtonen et al. 2014). Extending the length of time series, the frequency distribution changes of extreme values from the historical period (plus past1000) to the future2099 do not indicate a significant difference compared with those from the historical period to the future2099.

In the study, the results (Figs. 10, 11, and 13) show there is no significant trend for extreme precipitation in the past1000 period in Europe. This is similar with what is shown in the study of Landrum et al. (2013), which demonstrated that there were no statistically significant differences of effective precipitation (i.e., precipitation minus losses from evaporation, etc.) between the MCA (AD 900–1150) and LIA (AD 1500–1850) periods of the past1000 by using the last millennium simulations of CCSM4. To further verify the difference of precipitation between the MCA and LIA periods, we performed a *t* test to compare the annual precipitation of both periods from all the GCMs; the results show that there is no significant difference between those two periods in the five European regions. This is different from the study of Feurdean et al. (2015), which found that the MCA period was wetter than the LIA period from the multiproxy analysis by using the reconstructed data. It is well known that Europe has mostly a mild maritime climate and the sea temperature may have strong impact on precipitation in Europe. It would be helpful to understand the change of precipitation in past1000 if the change trends of the sea temperature were available for Europe. Xu et al. (2017) analyzed the variations of El Niño–Southern Oscillation (ENSO) and North Atlantic Oscillation (NAO) based on the outputs of the last millennium (850–1849) and historical experiments (1850–2005) from two climate models CCSM4 and MPI-ESM-P. The calculated Niño-3.4 indices from sea surface temperature displayed stable multicentennial fluctuations during the last millennium and a fast-increasing trend since 1900. This trend of sea surface temperature is similar as what we see from the precipitation during the past1000 in Europe.

This study attempted to examine whether the period covered by instrumental observations could represent extreme precipitation variability in a longer period including both past1000 and historical periods. First, we can see that almost all GCMs show no significant change in mean annual precipitation and maximum 1-day precipitation from the past1000 to the historical period for the majority of grid points in Europe based on the significance test (see Figs. 8 and 9). However, the maximum 1-day precipitation increases significantly from the historical period to the future2099 in most grid points of Europe. A previous study by Lehtonen et al. (2014) also stated that in regions of Europe where mean precipitation remains effectively unaltered, there is a statistically significant increase in the maximum 1-day precipitation. Besides, the precipitation distribution changes from the historical period to the future 2099 are slightly different from the changes from the past1000 plus the historical period to the future 2099 in all regions (see in Figs. 12 and 13). This can be seen from both annual precipitation and maximum 1-day precipitation. Therefore, there is no clear evidence for nonstationary precipitation extremes in Europe from the past1000 to the historical period in this study, although a greater range of extremes can be seen in a longer period. Lewis (2017) showed similar results, indicating no systematic difference in precipitation extremes with increasing length of time series (1000 year) compared to the observed values (100 year). Our results indicate that the period encompassed by around 100 years of instrumental records captures the precipitation variability and distribution of past 1000 years in Europe, although there are uncertainties from the CMIP5 GCMs, of which only five available members are used in this study.

6. Conclusions

This study has explored the characteristics of precipitation extremes and their changes over 1250 years (from the past1000 to the future2099) in Europe using CMIP5 experiments. Observations and model simulations of the historical experiment as well as proxy reconstructions and past1000 simulations in overlapping periods were compared.

The following conclusions can be drawn:

- When comparing the model-simulated precipitation with observations (ECA&D), CMIP5 GCMs tend to overestimate mean precipitation with the exception of southern Europe and underestimate the magnitude and frequency of extreme precipitation over most regions of Europe.
- In general, the annual precipitation and extreme precipitation tend to increase in the future from all GCM projections over most regions of Europe although the change from the RCP8.5 is much larger than that from the RCP2.6 scenario. Southern Europe, however, exhibits a slight increase of extreme precipitation associated with a decrease of annual precipitation in the future.
- There was no systematic change of precipitation extremes in the five European regions from the past1000 to the historical period, while an extraordinary increase in the frequency and magnitude of extreme precipitation events is apparent in the future GCM projections, which indicates nonstationary extremes in Europe.
- A greater magnitude increase can be seen in 100- and 200-yr return period precipitation than in 5- and 10-yr return period precipitation. At the same time, short-duration extreme precipitation (e.g., 1-day precipitation) will most likely increase more than longer-duration extreme values (e.g., 15-day precipitation). This may lead to more extreme flooding in Europe under global warming scenarios.

Acknowledgments. This work was supported by National Key Research and Development Program (2017YFA0603702), the CHEX project and HordaFlom project (269682), and the Research Council of Norway (FRINATEK Project 274310). The authors would like to acknowledge the contribution of the World Climate Research Program Working Group on Coupled Modeling and would like to thank climate modeling groups for making available their respective climate model outputs.

REFERENCES

Alexander, L. V., and Coauthors, 2006: Global observed changes in daily climate extremes of temperature and precipitation. *J. Geophys. Res.*, **111**, D05109, https://doi.org/10.1029/2005JD006290.

Allen, M., and W. Ingram, 2002: Constraints on future changes in climate and the hydrologic cycle. *Nature*, **419**, 228–232, https://doi.org/10.1038/nature01092.

Barcikowska, M. J., S. B. Kapnick, L. Krishnamurty, S. Russo, A. Cherchi, and C. K. Folland, 2020: Changes in the future summer Mediterranean climate: Contribution of teleconnections and local factors. *Earth Syst. Dyn.*, **11**, 161–181, https://doi.org/10.5194/ESD-11-161-2020.

Beniston, M., and Coauthors, 2007: Future extreme events in European climate: An exploration of regional climate model projections. *Climatic Change*, **81**, 71–95, https://doi.org/10.1007/s10584-006-9226-z.

Bothe, O., J. H. Jungclaus, and D. Zanchettin, 2013: Consistency of the multi-model CMIP5/PMIP3-past1000 ensemble. *Climate Past*, **9**, 2471–2487, https://doi.org/10.5194/cp-9-2471-2013.

Chan, S. C., E. J. Kendon, H. J. Fowler, S. Blenkinsop, and N. M. Roberts, 2014a: Projected increases in summer and winter UK sub-daily precipitation extremes from high-resolution regional climate models. *Environ. Res. Lett.*, **9**, 084019, https://doi.org/10.1088/1748-9326/9/8/084019.

——, ——, ——, ——, ——, and C. A. T. Ferro, 2014b: The value of high-resolution Met Office regional climate models in the simulation of multihourly precipitation extremes. *J. Climate*, **27**, 6155–6174, https://doi.org/10.1175/JCLI-D-13-00723.1.

Christensen, J. H., M. A. D. Larsen, O. B. Christensen, M. Drews, and M. Stendel, 2019: Robustness of European climate projections from dynamical downscaling. *Climate Dyn.*, **53**, 4857–4869, https://doi.org/10.1007/s00382-019-04831-z.

Coles, S., L. R. Pericchi, and S. Sisson, 2003: A fully probabilistic approach to extreme rainfall modeling. *J. Hydrol.*, **273**, 35–50, https://doi.org/10.1016/S0022-1694(02)00353-0.

Dai, E., Z. Wu, Q. Ge, W. Xi, and X. Wang, 2016: Predicting the responses of forest distribution and aboveground biomass to climate change under RCP scenarios in southern China. *Global Change Biol.*, **22**, 3642–3661, https://doi.org/10.1111/gcb.13307.

Donat, M. G., and Coauthors, 2013: Updated analyses of temperature and precipitation extreme indices since the beginning of the twentieth century: The HadEX2 dataset. *J. Geophys. Res. Atmos.*, **118**, 2098–2118, https://doi.org/10.1002/JGRD.50150.

Efron, B., 1969: Student's *t*-test under symmetry conditions. *J. Amer. Stat. Assoc.*, **64**, 1278–1302, https://doi.org/10.2307/2286068.

Feurdean, A., and Coauthors, 2015: Last millennium hydro-climate variability in central-eastern Europe (northern Carpathians, Romania). *Holocene*, **25**, 1179–1192, https://doi.org/10.1177/0959683615580197.

Fowler, H. J., and C. G. Kilsby, 2003: A regional frequency analysis of United Kingdom extreme rainfall from 1961 to 2000. *Int. J. Climatol.*, **23**, 1313–1334, https://doi.org/10.1002/joc.943.

——, M. Ekström, S. Blenkinsop, and A. P. Smith, 2007: Estimating change in extreme European precipitation using a multimodel ensemble. *J. Geophys. Res.*, **112**, D18104, https://doi.org/10.1029/2007JD008619.

Gellens, D., 2002: Combining regional approach and data extension procedure for assessing GEV distribution of extreme precipitation in Belgium. *J. Hydrol.*, **268**, 113–126, https://doi.org/10.1016/S0022-1694(02)00160-9.

Groisman, P. Ya., R. W. Knight, D. R. Easterling, T. R. Karl, G. C. Hegerl, and V. N. Razuvaev, 2005: Trends in intense precipitation in the climate record. *J. Climate*, **18**, 1326–1350, https://doi.org/10.1175/JCLI3339.1.

Hirabayashi, Y., R. Mahendran, S. Koirala, L. Konoshima, D. Yamazaki, S. Watanabe, H. Kim, and S. Kanae, 2013: Global flood risk under climate change. *Nat. Climate Change*, **3**, 816–821, https://doi.org/10.1038/nclimate1911.

Hodnebrog, Ø., and Coauthors, 2019: Intensification of summer precipitation with shorter timescales in Europe. *Environ. Res. Lett.*, **14**, 124050, https://doi.org/10.1088/1748-9326/ab549c.

Huang, W. H., Y. Sui, X. G. Yang, S. W. Dai, and M. S. Li, 2013: Characteristics and adaptation of seasonal drought in southern China under the background of climate change. III. Spatiotemporal characteristics of seasonal drought in southern China based on the percentage of precipitation anomalies. *Chin. J. Appl. Ecol.*, **24**, 397–406.

Jenkinson, A. F., 1955: The frequency distribution of the annual maximum (or minimum) values of meteorological elements. *Quart. J. Roy. Meteor. Soc.*, **81**, 158–171, https://doi.org/10.1002/qj.49708134804.

Jiang, Z., W. Li, J. Xu, and L. Li, 2015: Extreme precipitation indices over China in CMIP5 models. Part I: Model evaluation. *J. Climate*, **28**, 8603–8619, https://doi.org/10.1175/JCLI-D-15-0099.1.

Kendon, E. J., N. M. Roberts, H. J. Fowler, M. J. Roberts, S. C. Chan, and C. A. Senior, 2014: Heavier summer downpours with climate change revealed by weather forecast resolution model. *Nat. Climate Change*, **4**, 570–576, https://doi.org/10.1038/nclimate2258.

Khaliq, M. N., T. B. M. J. Ouarda, J. C. Ondo, P. Gachon, and B. Bobée, 2006: Frequency analysis of a sequence of dependent and/or non-stationary hydrometeorological observations: A review. *J. Hydrol.*, **329**, 534–552, https://doi.org/10.1016/j.jhydrol.2006.03.004.

Kharin, V. V., F. W. Zwiers, X. Zhang, and G. C. Hegerl, 2007: Changes in temperature and precipitation extremes in the IPCC ensemble of global coupled model simulations. *J. Climate*, **20**, 1419–1444, https://doi.org/10.1175/JCLI4066.1.

Klein, F., H. Goosse, N. E. Graham, and D. Verschuren, 2016: Comparison of simulated and reconstructed variations in East African hydroclimate over the last millennium. *Climate Past*, **12**, 1499–1518, https://doi.org/10.5194/cp-12-1499-2016.

Klein Tank, A. M. G., F. W. Zwiers, and X. Zhang, 2009: Guidelines on analysis of extremes in a changing climate in support of informed decisions for adaptation. WCDMP-72, WMO/TD-1500, 56 pp.

Koutroulis, A., M. G. Grillakis, I. K. Tsanis, and L. Papadimitriou, 2016: Evaluation of precipitation and temperature simulation performance of the CMIP3 and CMIP5 historical experiments. *Climate Dyn.*, **47**, 1881–1898, https://doi.org/10.1007/s00382-015-2938-x.

Landrum, L., B. L. Otto-Bliesner, E. R. Wahl, A. Conley, P. J. Lawrence, N. Rosenbloom, and H. Teng, 2013: Last millennium climate and its variability in CCSM4. *J. Climate*, **26**, 1085–1111, https://doi.org/10.1175/JCLI-D-11-00326.1.

Lehtonen, I., K. Ruosteenoja, and K. Jylhä, 2014: Projected changes in European extreme precipitation indices on the basis of global and regional climate model ensembles. *Int. J. Climatol.*, **34**, 1208–1222, https://doi.org/10.1002/joc.3758.

Lenderink, G., and H. J. Fowler, 2017: Understanding rainfall extremes. *Nat. Climate Change*, **7**, 391–393, https://doi.org/10.1038/nclimate3305.

Lewis, S. C., 2017: Assessing the stationarity of Australian precipitation extremes in forced and unforced CMIP5 simulations. *J. Climate*, **31**, 131–145, https://doi.org/10.1175/JCLI-D-17-0393.1.

Ljungqvist, F. C., P. J. Krusic, H. S. Sundqvist, E. Zorita, G. Brattström, and D. Frank, 2016: Northern Hemisphere hydroclimate variability over the past twelve centuries. *Nature*, **532**, 94–98, https://doi.org/10.1038/nature17418.

Madsen, H., D. Lawrence, M. Lang, M. Martinkova, and T. R. Kjeldsen, 2014: Review of trend analysis and climate change projections of extreme precipitation and floods in Europe. *J. Hydrol.*, **519**, 3634–3650, https://doi.org/10.1016/j.jhydrol.2014.11.003.

Martel, J., A. Mailhot, and F. Brissette, 2020: Global and regional projected changes in 100-year subdaily, daily, and multiday precipitation extremes estimated from three large ensembles of climate simulation. *J. Climate*, **33**, 1089–1103, https://doi.org/10.1175/JCLI-D-18-0764.1.

Matthews, J. A., and K. R. Briffa, 2005: The "Little Ice Age": Re-evaluation of an evolving concept. *Geograf. Ann.*, **87A**, 17–36, https://doi.org/10.1111/j.0435-3676.2005.00242.x.

Merz, B., F. Elmer, M. Kunz, B. Mühr, K. Schröter, and S. Uhlemann-Elmer, 2014: The extreme flood in June 2013 in Germany. *Houille Blanche*, **1**, 5–10, https://doi.org/10.1051/lhb/2014001.

Min, S. K., X. Zhang, F. W. Zwiers, and G. C. Hegerl, 2011: Human contribution to more intense precipitation extremes. *Nature*, **470**, 378–381, https://doi.org/10.1038/nature09763.

Pauling, A., J. Luterbacher, C. Casty, and H. Wanner, 2006: Five hundred years of gridded high-resolution precipitation reconstructions over Europe and the connection to large-scale circulation. *Climate Dyn.*, **26**, 387–405, https://doi.org/10.1007/s00382-005-0090-8.

Peters, G. P., and Coauthors, 2012: The challenge to keep global warming below 2°C. *Nat. Climate Change*, **3**, 4–6, https://doi.org/10.1038/nclimate1783.

Prein, A. F., R. M. Rasmussen, K. Ikeda, C. Liu, M. P. Clark, and G. J. Holland, 2017: The future intensification of hourly precipitation extremes. *Nat. Climate Change*, **7**, 48–52, https://doi.org/10.1038/nclimate3168.

Rajczak, J., and C. Schar, 2017: Projections of future precipitation extremes over Europe: A multimodel assessment of climate simulations. *J. Geophys. Res. Atmos.*, **122**, 10 773–10 800, https://doi.org/10.1002/2017JD027176.

Ruosteenoja, K., J. Kirsti, R. Jouni, and M. Antti, 2017: Surface air relative humidities spuriously exceeding 100% in CMIP5 model output and their impact on future projections. *J. Geophys. Res. Atmos.*, **122**, 9557–9568, https://doi.org/10.1002/2017JD026909.

Schindler, A., A. Toreti, M. Zampieri, E. Scoccimarro, S. Gualdi, S. Fukutome, E. Xoplaki, and J. Luterbacher, 2015: On the internal variability of simulated daily precipitation. *J. Climate*, **28**, 3624–3630, https://doi.org/10.1175/JCLI-D-14-00745.1.

Scoccimarro, E., S. Gualdi, A. Bellucci, M. Zampieri and A. Navarra, 2016: Heavy precipitation events over the Euro-Mediterranean region in a warmer climate: Results from CMIP5 models. *Reg. Environ. Change*, **16**, 595–602, https://doi.org/10.1007/s10113-014-0712-y.

Shi, J., Q. Yan, D. Jiang, J. Min, and Y. Jiang, 2016: Precipitation variation over eastern China and arid central Asia during the past millennium and its possible mechanism: Perspectives from PMIP3 experiments. *J. Geophys. Res. Atmos.*, **121**, 11 989–12 004, https://doi.org/10.1002/2016JD025126.

Trenberth, K., and Coauthors, 2007: Observations: Surface and atmospheric climate change. *Climate Change 2007: The Physical Science Basis*, S. Solomon et al., Eds., Cambridge University Press, 235–336.

Ulbrich, U., T. Brü, A. H. Fink, G. C. Leckebusch, A. Krüger, and J. G. Pinto, 2003: The central European floods of August 2002: Part 1—Rainfall periods and flood development. *Weather*, **58**, 371–377, https://doi.org/10.1256/wea.61.03A.

van den Besselaar, E. J. M., A. M. G. Klein Tank, and T. A. Buishand, 2013: Trends in European precipitation extremes over 1951–2010. *Int. J. Climatol.*, **33**, 2682–2689, https://doi.org/10.1002/JOC.3619.

Wei, J., and J. G. Ma, 2003: Comparison of palmer drought severity index, percentage of precipitation anomaly and surface humid index. *Acta Geogr. Sin.*, **58**, 117–124.

Westra, S., L. V. Alexander, and F. W. Zwiers, 2013: Global increasing trends in annual maximum daily precipitation. *J. Climate*, **26**, 3904–3918, https://doi.org/10.1175/JCLI-D-12-00502.1.

Willett, K., P. Jones, N. Gillett, and P. Thorne, 2008: Recent changes in surface humidity: Development of the HadCRUH dataset. *J. Climate*, **21**, 5364–5383, https://doi.org/10.1175/2008JCLI2274.1.

Xu, T. T., Z. G. Shi, and Z. S. An, 2017: Responses of ENSO and NAO to the external radiative forcing during the last millennium: Results from CCSM4 and MPI-ESM-P simulations. *Quat. Int.*, **487**, 99–111, https://doi.org/10.1016/J.QUAINT.2017.12.038.